ABSTRACT

Title of Document:	NANOCHANNEL FABRICATION USING THERMOMECHANICAL DEFORMATION OF THERMOPLASTICS
	Kapil Sahasrabudhe, M.S. Mechanical Engineering, September 2006
Directed By:	Dr. Donald L. DeVoe, Associate Professor, Department of Mechanical Engineering

Nanofluidics has been a major field of research for application in areas like single molecule detection. Most of the research efforts have been concentrated in developing novel nanochannel fabrication techniques. Most of these fabrication techniques developed are either expensive or time consuming.

A novel, low-cost fabrication technique to generate sub-micrometer wide channels in thermoplastic chips with potential application in single molecule detection is demonstrated. This nanochannel fabrication technique is based on thermo-mechanical deformation of a section of microchannel in thermoplastic chip to nanometer dimensions. A custom, mechanical rig was designed, fabricated and optimized to produce a pre-defined thermo-mechanical deformation in thermo-plastic microchannel chips. Rectangular microchannels with different shapes and sizes were deformed using this rig to optimize the initial microchannel dimensions. Low aspect ratio (height:width) channels with smaller initial dimensions exhibit more potential to reach sub-micrometer widths. However, the nanochannel fabrication consistency was adversely affected by manufacturing and assembly tolerances.

NANOCHANNEL FABRICATION USING THERMOMECHANICAL DEFORMATION OF THERMOPLASTICS

By

Kapil Sahasrabudhe

Thesis submitted to the Faculty of the Graduate School of the
University of Maryland, College Park in partial fulfillment
of the requirements for the degree of
Master of Science,
Mechanical Engineering
2006

Advisory Committee:

Dr. Donald L. DeVoe, Associate Professor of Mechanical Engineering (Chair)
Dr. Doug S. English, Assistant Professor of Chemistry and Biochemistry
Professor Patrick F. McCluskey, Associate Professor of Mechanical Engineering

Dedication

To my late parents, who have always been my source of inspiration.

Acknowledgements

My words fail to express my deep gratitude to my advisor Dr. Donald DeVoe for his invaluable guidance and support. He has been an excellent source of motivation. I extend my thanks to Dr. Patrick McCluskey and Dr. Doug English for directing me and giving invaluable suggestions on this thesis. I would also take this opportunity to thank Dr. Akshay Naik for his constant support and help in capturing the SEM images.

I sincerely thank my friends Lou Hromada, Likun Zhu, Joy Yi, Wei-Jen, Kevin Tsao, Lihua Li, Parshant Kumar, Jake Yang, Chien-Fu Chen, Chen-Fei Kung, Karthik Chandrashekar, Ragunath Sankarnarayanan, Vishnucharan Arcot, Shirsho Sengupta, Jishnu Keshavan and all my friends at University of Maryland.

Tai, Shubhada, Ajeet, Shri, Aai, Bendre Kaka, Bendre Kaku: This thesis would not have been possible without your support.

Table of Contents

List of Figures

Chapter 1: Introduction

1.1 Background

After the success of integrated circuit (IC) technology during the later half of the 20th century, considerable amount of time and money has been spent on miniaturizing various macro-scaled technologies to create smaller, faster, efficient and more accurate systems. "Small is better" has been the motto of explorers in this area. Vacuum tubes in earlier era computers have been replaced by modern day microprocessors with faster computing power with a fraction of the original size. Recent additions to these technologies have been Micro Electro Mechanical Systems (MEMS) and Nanotechnology. Various mechanical sensors and actuators have been replaced by more precise, miniaturized and efficient micrometer-scaled actuators and sensors.

Fluidic systems have also tremendously benefited from this revolution, with the advent of micro and nanofluidics. Micro and nanofluidics is a multi-disciplinary field to design and develop micro and nano-scaled systems for fluid manipulation and control, used in various scientific investigations like bio-analysis. Microfluidics dates back to the early seventies when a miniature gas chromatograph was developed at Stanford University [32]. Substantial development has been achieved since then, with the minimum feature size going down to few nanometers along with the development of numerous fluid transportation and control techniques. Micro and Nanofluidics offer note-worthy advantages over their macro counterparts in terms of high-throughput, accuracy, sensitivity, size, lower sample volumes and understanding of molecular dynamics. Various costly and bulky fluidic systems are/will be replaced by compact and cost-effective micro and nano fluidic chips. By integrating micro and nanofluidic systems with

sensors, actuators and other electronics, numerous functions can be carried out on a single chip [21]. With smart geometries and novel fluid manipulation systems, performance of these systems can be enhanced in terms of process handling capability, through-put, accuracy etc. A perfect example of this trend is evident in lab-on-a-chip (LOC) or micro total analysis system technology, in which scientists are trying to integrate and miniaturize desktop laboratory procedures on hand-held micro and nanofluidic chips. Although in its early stages, micro and nanofluidics holds a potential to grow into a path-breaking technology and promise to provide a big opportunity for commercialization. These technologies have already found application in various fields such as biotechnology, chemistry and engineering.

The need for such smaller and efficient fluidic systems has called for novel and effective fabrication techniques. Scientists and researchers around the world have adopted a philosophy "Let a thousand flowers bloom"[†], which has resulted in a variety of nanofabrication methods to produce micro and nanochannels in silicon, glass and polymers. Each fabrication method is capable of producing micro and/or nanoscale channels, however some methods are time-consuming while some are costly or require expensive machines/equipments. Thus these methods are not suitable for large-scale production. Thus, there has always been a need to quickly produce nano-scaled channels at a relatively low-cost. The following section will discuss some of the common fabrication techniques used to develop nanochannels.

[†] Term coined by Whitesides et al. [34]

1.2 Current Nanochannel Fabrication Techniques[‡]

Nanofabrication techniques can be broadly classified into two main categories based on the approach taken for fabrication, namely; top-down and bottom-up methods (Fig. 1.1). Top-down methods perform large scale patterning and reducing feature dimensions to nanoscale while bottom-up methods rely on specific arrangement of atoms and molecules to create nanostructures [34].

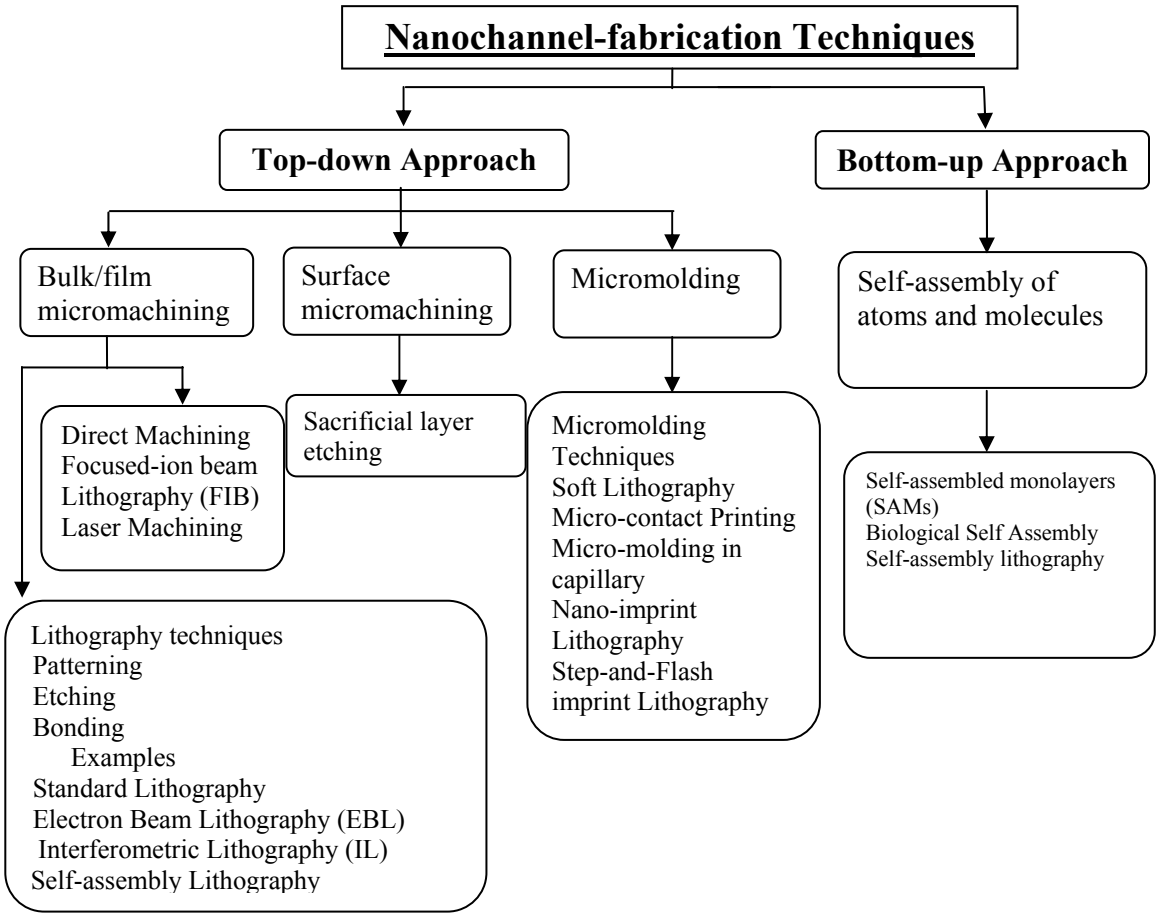

Figure 1.1 Classification of various nanochannel fabrication techniques.

[‡] Mijatovic et al provide an excellent review of various fabrication technologies for nanofluidic system and has been a major source of information for this section [21]

1.2.1 Top-down Approach

As the name suggests, in top-down approach nanoscale features are built by machining into a material from top to bottom. This approach can be further classified into three sub-categories [21]:

- Bulk/film micromachining
- Surface micromachining
- Mold micromachining

1.2.1.1 Bulk/Film Micromachining

In bulk/film micromachining of nanochannels, a channel is etched into a substrate wafer (bulk micromachining) or a thin (few nanometers thick) film deposited on a wafer (film micromachining). This is performed with standard lithography or other advanced lithography methods. The use of lithographic techniques to produce nano-scaled structures is known as nanolithography. A photoresist (organic polymer) is spin-coated on the surface of a substrate or on a thin film deposited on the substrate. A mask with negative of the pattern to be developed on the photoresist is aligned on the resist. The resist is then exposed to ultraviolet (UV) light of suitable wavelength (typically ~ 250 nm for standard lithography) through the mask. The exposed photoresist then can be selectively removed using an appropriate developer solution. The underlying thin film or the substrate can be subsequently wet or dry etched to form an open nanotrench. This nanotrench is then covered with another substrate with access holes to form an enclosed nanochannel.

Various bonding or sealing methodologies are explained later in this section. Fig. 1.2 shows a schematic of the fabrication process flow in standard lithography.

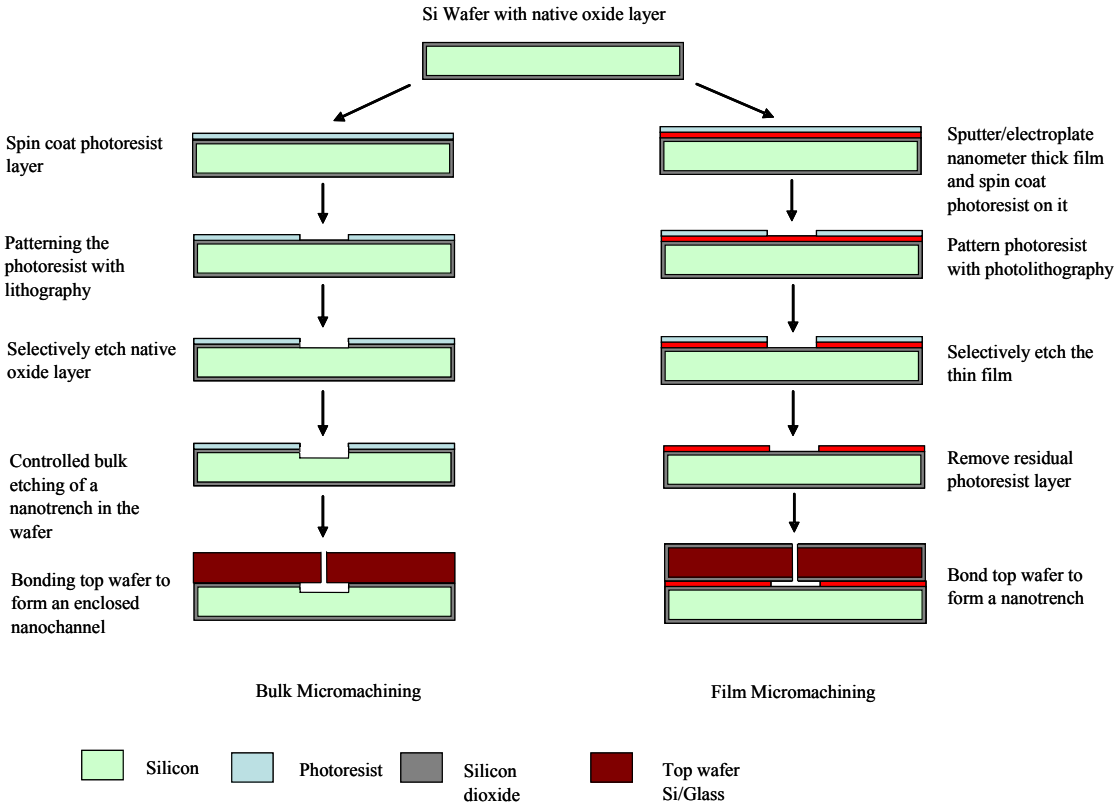

Figure 1.2 Fabrication process flow in bulk and film micromachining [21]

Standard photolithography techniques have been consistently used to mass-produce channels with widths measuring few micrometers. However, the widths of the channels are limited by the resolution of the photolithographic process used. Typical UV light used in conventional photolithography has a wavelength of around 250 nm. For fabrication of channels with widths less than half of this wavelength, conventional photolithography cannot be used as diffraction will cause blurred features [21]. On the other hand, various technological developments in instruments used in lithography have made it possible to fabricate features in the order of 70 nm with custom experimental setup and about 100 nm in mass production [34] [1]. But these developments have made

the process expensive. To reduce the blurring effects due to diffraction and still achieve extremely narrow channel widths, light with extremely small wavelength must be used. X-rays or extreme UV light with smaller wavelengths can be used for this purpose [5] [23]. But conventional lenses are opaque to extreme UV light and cannot focus X-rays. Moreover, the high energies of these rays can damage most of the materials used in masks and lenses, which is not acceptable [21].

A simple way of getting around the above-mentioned limitations of using standard lithography to get extremely narrow channels is developing nanometer high channels rather than nanometer wide channels, by controlling the etch depth into a substrate or by simply etching away nanometer thick layers deposited on a substrate. Channels thus developed can be further sealed to form enclosed structures. Mao et al have demonstrated fabrication of 20 nm high planar nanofluidic channels in silicon and glass with standard lithography and dry and wet etching [20]. Similarly, Kutchoukov et al have fabricated shallow nanochannels in glass with anodic bonding technique and also with integrated polysilicon electrodes [17] [18]. Similarly, Haneveld et al have demonstrated fabrication of fluidic 1D nanometer deep (20 nm) channel by controlled wet etching [9].

Various other nanolithography technologies have also been developed to eliminate the use of mask, a limiting factor in nanochannel development. Electron beam lithography (EBL) and focused-ion beam lithography (FIB) are the two most important techniques in this arena. A note-worthy advantage of these methods is that extremely narrow nanochannels, to the order of 10 nm can be developed by controlling the beam widths [21]. In EBL, required pattern is directly written in a photoresist layer using a

focused electron beam [34]. In case of negative photoresist such as SU8*, the unexposed photoresist is removed using a suitable resist developer leaving behind nano-scaled resist structures. In case of a positive photoresist like PMMA, the pattern written by electron beam is removed after development. Positive photoresist patterned with EBL is used as a masking layer for wet or dry etching of nanotrenches in substrates or deposited films. Thus, requirement of special materials and technologies to get few nanometer (~100 nm) wide channels using standard nanolithography can be eliminated by EBL. However, pattern writing using electron beam is a serial process making it expensive and time-consuming and hence unsuitable for large-scale production. Moreover, a major drawback of EBL is the proximity effect caused due to electron scattering in the resist. When the electron beam hits the photoresist surface, the electrons undergo elastic (angle change and no energy loss) and in-elastic (energy loss) collisions. The elastically collided electrons that rebound back to the source are called back-scattered electrons and the in-elastically collided electrons further produce secondary electrons, Auger electrons and X-rays to compensate for the energy loss. The back-scattered electrons cause the features written by the electron beam to be wider in densely patterned areas. This limits resolution and contrast [4]. Chen et al have demonstrated 5-7 nm wide etched lines in Si substrate using polymethyl methacrylate (PMMA) resist [6]. These etched lines can be capped to form enclosed nanochannels. Bilenberg et al have used EBL to develop sub-30 nm wide photoresist structures, which are then transferred to underlying Si wafer by dry etching [3]. Mali et al have used electron beam to directly fabricate enclosed microchannels by varying the beam energy and dosage [19].

FIB uses focused Ga ions to directly machine a thin film or a substrate. Thus, use of photoresist is not required and features with widths matching the beam width can be developed. However, FIB can cause mechanical damage during direct milling and can also produce Ga ion doping of the material [1]. Kaige et al have employed FIB to fabricate 75 nm wide and 100 nm high silicon nitride nanofluidic channel array [12]. Based on the similar concept, Shao et al have used focused proton beam to directly write high aspect ratio sub-micrometer channels in PMMA and then thermally bond another PMMA layer to form enclosed nanochannel structure [27]. Laser etching is another technique to directly develop nano-scaled channels in materials. Mullenborn et al have used continuous wave laser to fabricate 70 nm wide trenches in silicon wafer in chlorine environment [22]. These trenches can be further covered with another silicon wafer to form enclosed nanochannel.

Another lithographic technique to get well-arranged nanochannels is interferometric lithography (IL). This maskless technique makes use of two or more coherent beams to produce interference pattern on a photoresist, which when developed produces well-spaced nanostructures with regular pitch and widths. Thus, nanochannels can be produced on large areas with varied feature dimensions (pitch and channel width). IL is an in-expensive and quick patterning method that is well-suited for high-throughput manufacturing. In this method, the two coherent beams with wavelength λ are crossed at an angle 2θ. The optical path difference between these interfering beams produces an interference pattern with period given by $d = \lambda / (2 \sin\theta)$. Thus by tuning the wavelength or the angle between the interfering beams, period of interference pattern can be varied along with the structure widths. With the use of regular UV light, periods on the order of

hundreds of nm and features in sub-100 nm range can be produced, well-beyond the conventional optical lithography limitations. Moreover, use of deeper UV light and immersion techniques can further scale down periods to sub-100 nm and feature sizes to around 10 nm [21]. O'Brien II et al have fabricated an integrated nanofluidic chip using interference lithography [25].

Self assembly lithography is the process of developing a lithography mask, with nanometer resolution, by formation of self-assembled structures. Further etching using this mask can produce nanoscaled structures in a substrate. This is an efficient and low-cost approach to create nanochannels well-below photographic resolution limits (~ 100 nm) [8] [26]. A diblock co-polymer is used in place of conventional photoresist. A diblock polymer consists of molecules of two covalently bonded immiscible polymer blocks. The molecular structure of the polymer prevents macro-scale phase separation, however causes a micro-level phase separation producing self assembled structures on minority polymer blocks. These self-assembled structures resemble pattern on a mask. This micro-scaled re-arrangement occurs when the diblock polymer is heated above the glass transition temperature of both polymer blocks. For example, in a diblock polymer consisting of polystyrene and polymethyl methacrylate (PMMA) as its constituent blocks, microphase separation produces hexagonal lattice of PMMA cylinders in a matrix of polystyrene. PMMA is then etched away by exposure to UV light and development process. Thus, features ranging from hundreds of nanometers to below 10 nm can be achieved and use of high resolution nanolithography is eliminated [21].

A combined approach is also demonstrated to develop nano-scaled features by merging the principles of lithography and self-assembly called the hybrid method. Kim et al have demonstrated epitaxial self-assembly of diblock co-polymers on lithographically patterned substrates to produce defect-free, regular and periodic patterns over arbitrarily large areas (Fig. 1.3). In this approach, the nano-scaled structures produced are determined by the size and quality of the lithographically defined topological pattern rather than inherent limitations of self-assembly process.

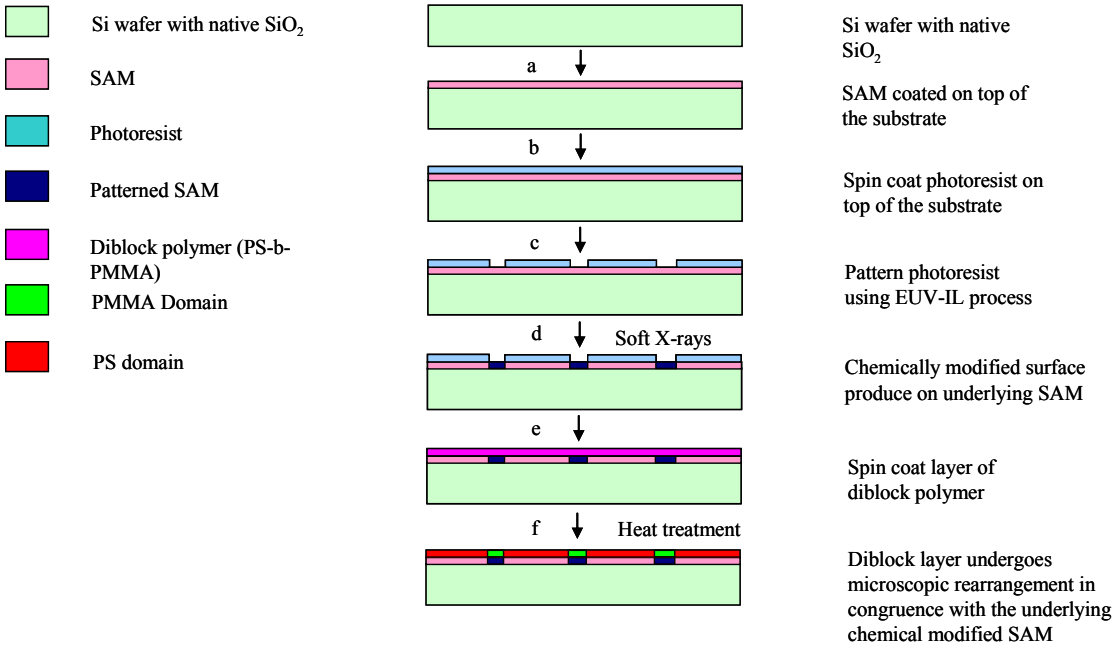

Figure 1.3 Fabrication process flow for epitaxial self assembly of diblock co-polymers [14]

The authors have presented a two step process to develop regular, periodic nanostructures of a diblock polymer, poly(styrene-block-methyl methacrylate) ((PS-b-PMMA), 104 kg/mol^{-1}, lamellar period approximately 48 nm) (Fig. 1.3). In this process a lithographically defined pattern in photoresists was used to develop a chemically

modified pattern in SAM. This chemically modified monolayer was used to microscopically rearrange the diblock polymer to create these nano-scaled patterns.

A Si wafer with native oxide layer was coated with a self-assembled monolayer (SAM) (Step a). A layer of photoresist was then spin coated on the monolayer (Step b). Photoresist was then pattern with alternating lines and spaces with periods between 45 nm and 55 nm using extreme ultraviolet interferometric lithography (EUV-IL) (Step c) The exposed underlying SAM was then chemically modified by irradiating soft X-rays in the presence of oxygen to produce polar groups on it's surface (Step d). The photoresist was then removed with repeated solvent treatment. A symmetric, lamella-forming PS-b-PMMA diblock polymer of period 48 nm was spin-coated on this pattern SAM (Step e). Wafer with the epitaxial layers was then annealed above the glass transition temperatures of individual blocks of the co-polymer to diblock copolymer morphologies. The polar groups on the chemically modified SAM provided a surface for preferential wetting by PMMA block and unmodified region exhibit neutral wetting behavior by the block copolymer [14].

Stoykovich et al have extended this approach to develop non-regular patterns by self assembly of copolymer blends. Instead of just using a diblock copolymer, a ternary blend of diblock copolymers and homopolymers was used to create these non-regular structures. A ternary PS-b-PMMA/PS/PMMA blend was used for this purpose. The fabrication process essentially remains the same with the SAM being replaced by a poly-styrene brush [29].

1.2.1.2 Surface Micromachining

In surface micromachining nano-scaled structures are developed on the surface of a wafer by selective deposition and etching. A bottom layer is first deposited on the surface of a wafer. A nanometer thick sacrificial layer is deposited on the bottom layer and patterned. This sacrificial layer will be etched later to obtain an enclosed structure. A top layer is deposited over the sacrificial layer and patterned to provide access holes for the etchant to reach the underlying sacrificial layer. A nanochannel is thus formed by etching away the underlying sacrificial layer (Fig. 1.4). It can be seen that this approach is similar to film micromachining.

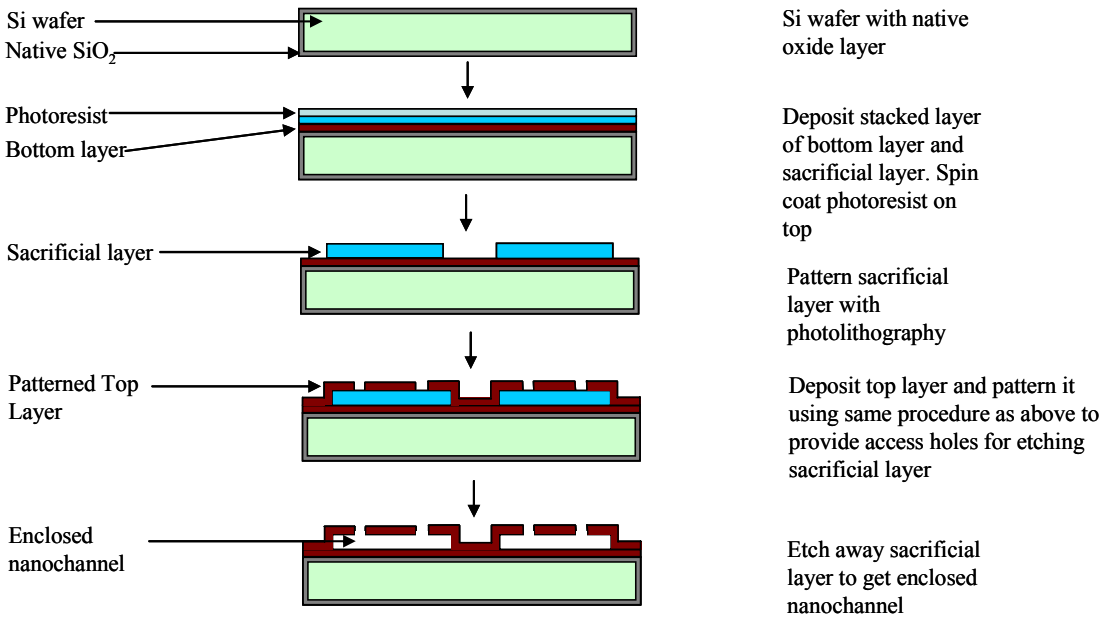

Figure 1.4 Fabrication process flow in surface micromachining of nanochannels [21].

The bottom layer is not always required and the sacrificial layer can be directly deposited on the surface of the substrate. But a bottom layer is deposited to form the nanochannel of the same material. If the top and bottom surfaces of the channel are

not of the same material, then the fluid flow in the channel can be affected depending upon the nature of the materials that form the channel. Polysilicon is a common sacrificial material but a thermally degradable material can also be used [21] [33]. The main disadvantage of this method is the large amount of time required to etch the underlying sacrificial layer and is therefore not suited for fabricating long channels. Moreover, special access holes are required for the etchant to reach the sacrificial material. Nanostructures can also be damaged during wet etching by the drag forces and also by stiction during drying. Dry etching is a good alternative for wet etching to produce uniform structures without damage [21].

1.2.1.3 Mold Micromachining

In mold micromachining, a mold in the inverse shape of the required structure is developed. This mold is then filled with a structural material and later the mold is etched/removed leaving the desired structure behind in the structural material (Fig.1.5).

Poly(dimethylsiloxane) (PDMS) is an example of such structural material. Generation of a PDMS stamp is a quick and easy process and does not require clean-room environment and is performed by soft lithography. In soft lithography process, the mold is produced by lithographically developing a pattern (master) in a photoresist or wet/dry etching a pattern in a Si wafer that is used as a template. The pattern is negative of the required pattern in PDMS. PDMS, which is an elastomer is poured on the master template and cured in an oven. After curing, PDMS forms a rubber-like solid which can be easily peeled off the master template leaving behind an imprint from the template (Fig.1.5). This imprinted PDMS layer can then be covered with another flat PDMS layer

to form an enclosed structure like a nanochannel. Soft lithography is a good option for rapid prototyping.

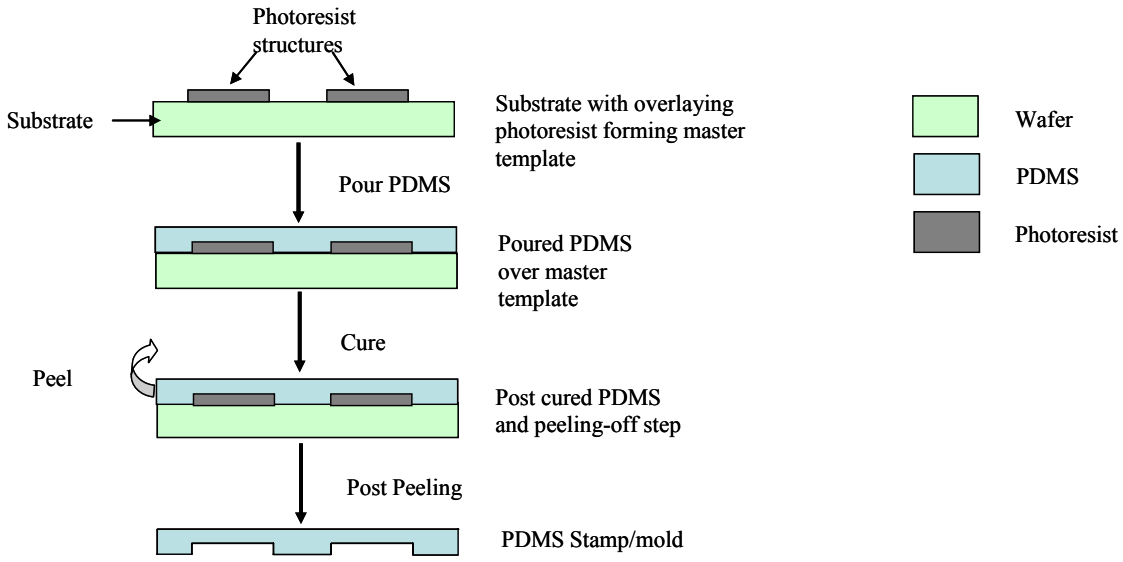

Figure 1.5 Fabrication process flow in soft lithography [34].

However generation of the master with nanoscaled structures requires use of expensive techniques such as electron-beam lithography. Fabrication of PDMS stamp from master template is cheap and easy process. This PDMS stamp or mold can be further employed for microcontact printing and micromolding in capillaries.

In micro-contact printing, the developed PDMS stamp is used as a stencil to transfer its pattern to a surface in contact. In this process, the PDMS stamp is dipped in a solution containing organic molecules and brought into contact with a gold layer on a Si substrate with some applied pressure. These organic molecules are transferred to the gold forming a self-assembled monolayer (SAM) thus reproducing stamp's pattern (Fig. 1.6)

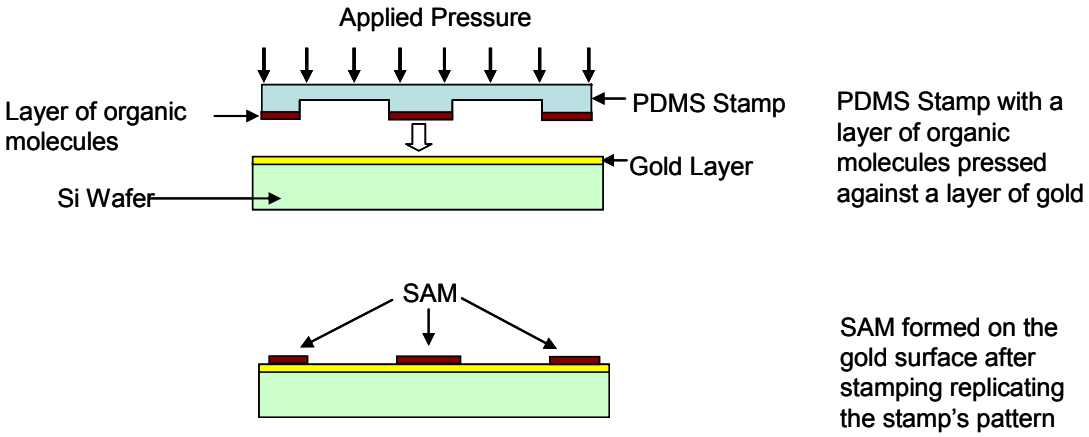

Figure 1.6 Fabrication process flow in micro-contact printing [21].

On the other hand, in micromolding in capillaries method, the PDMS is placed on hard surface like a glass substrate. A liquid polymer is then passed through the recesses between the stamp and the hard surface by capillary force. The liquid polymer nicely fills all the gaps between the two surfaces. When the liquid polymer solidifies, the PDMS mold can be peeled-off and a molded structure remains behind (Fig.1.7) [13].

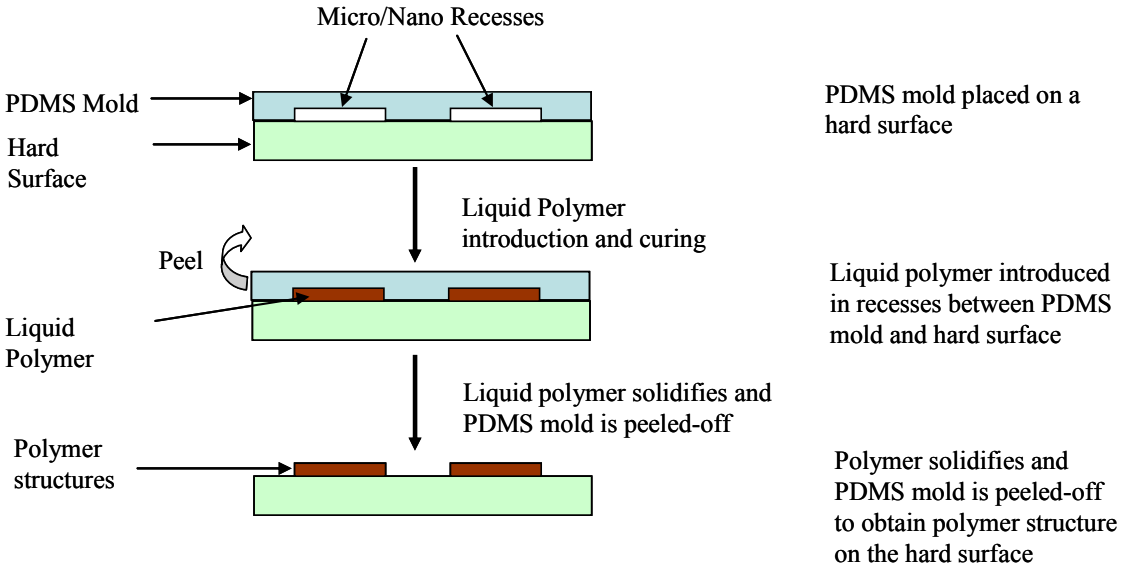

Figure 1.7 Fabrication process flow in micro-molding process [21].

PDMS is a soft elastomer and therefore prone to deformations and distortions that can lead to errors in the replicated pattern and/or misalignment of the pattern, hence not useful for complex structures [21]. This disadvantage can be overcome by methods such as step-and-flash imprint lithography and nanoimprint lithography (NIL). In NIL, desired nano-scaled structure is embossed into a photoresist, which is then selectively etched to form the desired pattern on the substrate. A thin layer of photoresist is spin-coated on the surface of a substrate. A rigid mold is then pressed against this photoresist layer and whole assembly is heated above the resist's glass transition temperature. This embosses the mold pattern into the resist layer. The residual resist in the thin compressed area can then be selectively etched away. Thus a pattern in the resist is developed that mimics the master (Fig.1.8) [7]. The master mold can be developed using any of the above-mentioned nano-lithographic techniques. NIL is a fast process well-suited for large-scale production.

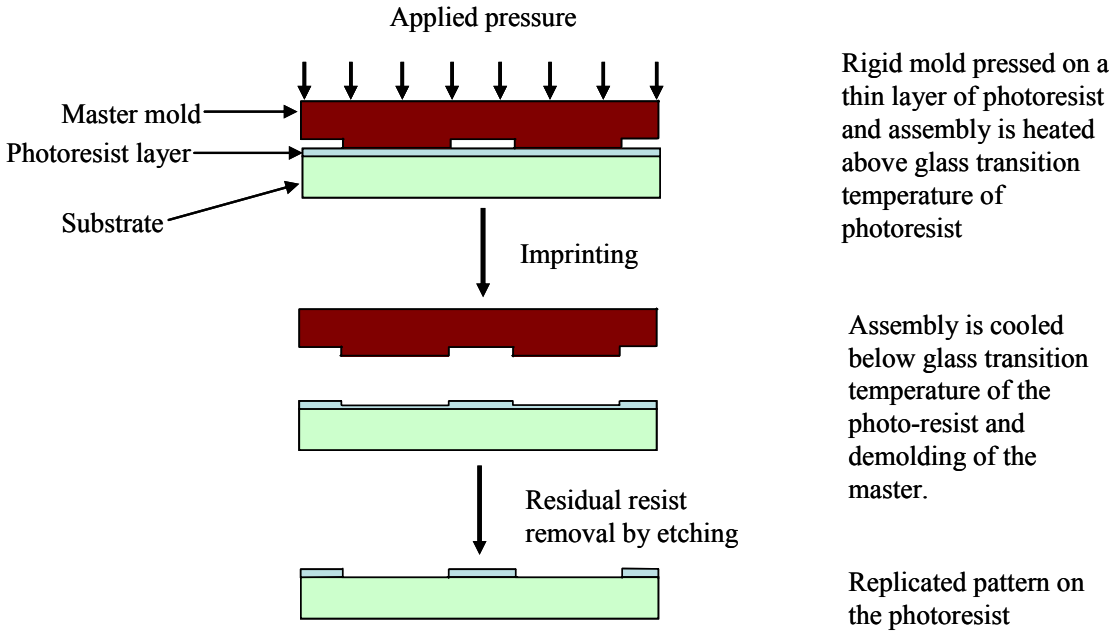

Figure 1.8 Fabrication process flow in nano-imprint lithography [7].

Features around 20 nm have been reported using NIL [1]. However, the fabrication of master mold is often expensive and any change in the pattern design required a complete new master mold, which is not economical. Moreover, NIL has limitation imprinting micro-scale and nano-scale patterns simultaneously.

1.2.2 Bottom-up Approach

Bottom-up approach relies on systematic assembly of atoms and molecules to form nanostructures through carefully controlled chemical reactions. This is a fairly recent approach and promises to provide cheaper alternative to top-down methods discussed above. Bottom-up approach has been used to fabricate structures like quantum dots and carbon nanotubes [21].

Quantum dots are crystals composed of few hundred molecules, which emit different wavelengths of light when exited with UV-rays, depending on their size. This property has resulted in use of quantum dots as bio-markers. A procedure to create quantum dots consists of a chemical reaction between a metal ion like cadmium and a molecule that can donate a selenium ion. This chemical reaction initiates simultaneous growth of numerous cadmium selenide nanocrystals. In order to prevent these crystals in lumping together to from a macro crystal, the chemical reaction is carried out in presence of organic molecules that act as surfactants, by coating the surface of each cadmium selenide crystal when it grows to a required size. Thus, the chemical reactions initiates growth of cadmium selenide crystals and when they grow a specific size, the organics molecules coat the crystals to form dots. The size of the dots can be controlled by controlling the reaction time. The geometry of the dots can be controlled to some extent

by use of different ratios of the organic molecules. Variety of shapes of dots such as spheres, rods and tetrapods can be created [34].

Carbon nanotubes are graphene cylindrical tubes several nanometers in diameter. These nanotubes can be produced by evaporation of solid carbon in an arc discharge, laser ablation and chemical vapor deposition (CVD) techniques. The structural properties of carbon nanotubes depend on the development process. For example, carbon nanotubes produced by evaporation and laser ablation are in the form of porous membranes and powders that requires further processing, whereas carbon nanotubes can be directly grown on substrates using CVD. Carbon nanotubes with sub-10 nm diameters can be produced. These nanotubes can be used as sacrificial structures to develop enclosed nanochannels [37].

Researchers are also exploring the field of developing nanostructures from colloids (nanoparticles in suspension). Xia et al have demonstrated an approach to fabricated nanoscale channels of silica nanoparticles by combining interference lithography and bottom-up approach of self-assembling colloidal silica nanoparticles. Channels with heights and widths as small as 100 nm were developed using this approach. In this process, a layer of photoresist with underlying anti-reflection coating was patterned on a silicon substrate with interference lithography. Silica nanoparticle dispersion was spin coated in layers on this patterned surface. After each spin coating step, the silica nanoparticles self-assemble to form a monolayer. This stacked up monolayers completely enclose the photoresist structures. The resist structures were removed by thermal degradation at 800^{o}C for 1.5-2 hours leaving behind enclosed nanochannels [36] (Fig.1.9).

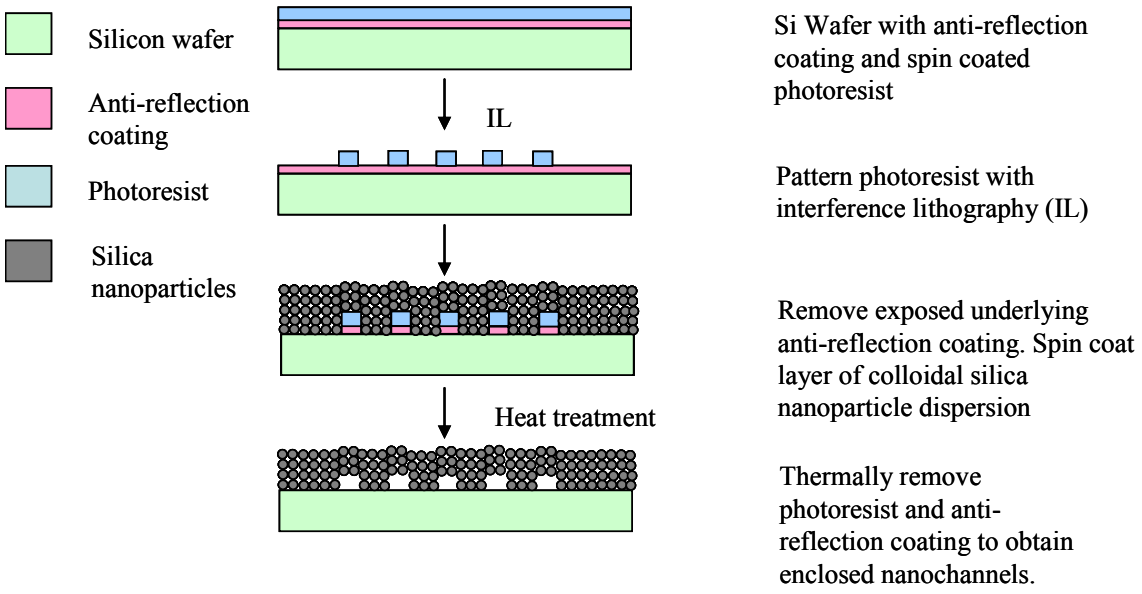

Figure 1.9 Fabrication of nanochannel by self-assembly of silica nanoparticles [36].

Biologically inspired self-assembly holds promise in bottom-up development of nanostructures. For instance, peptide nanotubes can be self-assembled from cylindrical octapeptides [21]. Self-assembling diblock polymers as explained above can also be use to fabricate nanostuctures by bottom-up approach.

1.2.3 Bonding

Bonding another substrate to a substrate containing nanotrench is an important step in completing fabrication of an enclosed nanochannel. Methods such as anodic bonding, fusion bonding, and thermal bonding are commonly employed to bond two wafers together. This section will briefly explain anodic and fusion bonding and other polymer bonding techniques. Thermal bonding of polymer nanofluidic chips will also be discussed.

1.2.3.4 Anodic Bonding

Anodic bonding is a process to bond a glass sheet to silicon wafer. In this process, the glass sheet is brought into contact with the silicon wafer. A high electric voltage is applied across this sandwich. The silicon wafer is kept at a positive potential relative to the glass. When the electric field is applied, positive ions from glass move towards the negative electrode producing a high electric field at the glass-silicon interface. This high electric field produces a large force that pulls the two surfaces together producing a strong bond. The whole process takes place at around 400^{o}C and voltage of the order of 1 kV is applied. Thus nanochannels can be developed in either

glass or silicon and a glass cover sheet can be anodically bonded to it to form an enclosed nanochannel [16].

1.2.3.5 Fusion Bonding

Fusion bonding is a process to attach two silicon or glass substrates together (Fig. 1.10). In this process, the surfaces of the substrates to be attached are made hydrophilic by creating hydroxyl groups on the attach surfaces.

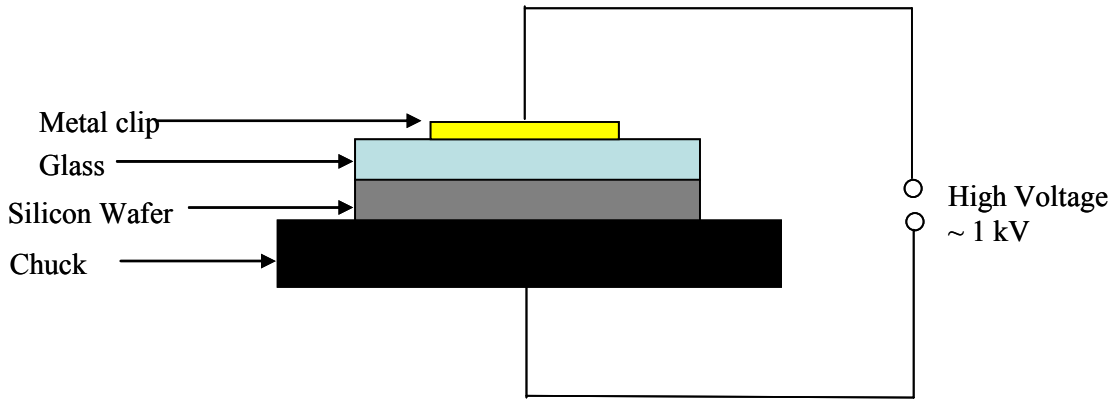

Figure 1.10 Fusion bonding process [16].

One way of doing this is boiling in nitric acid. Strong hydrogen bonds are formed when the substrates are brought into contact. The bonding process is carried out at a temperature between 300^{o}C to 800^{o}C. High operation temperatures between 800^{o}C to 1100^{o}C can be used to further strengthen the bond [16].

Apart from anodic and fusion bonding, thermal bonding of polymers is another commonly used technique to bond two polymer substrates. The polymer substrates are heated close to their glass transition temperature and pressed together to form a thermal bond. This procedure will be explained in-detail in chapter 3 as used in this fabrication process. It is absolutely essential to obtain a good bond in microfluidic

chips to prevent any leakage that can affect the performance of the chip. Two main factors affect the bond strength of thermally bonded polymer chips namely, bonding temperature and bonding force. These two factors are inversely proportional to each other. Bonding temperature is more important in terms of getting a good bond without collapsing the imprinted channel network during the bonding process. This is especially critical for imprinted channels with small heights. Reduction in height of the imprinted channel during the bonding process is also dependent on the aspect ratio of the channel. Tall and narrow channels are less prone to collapse than shallow and wide channels. In case of polymer wafers, the surfaces to be bonded together can be UV-ozone treated to create hydrophilic groups on the surfaces, which enhance the bond. Thus, the treated plastic wafers can be bonded at a temperature much lower than the glass-transition temperature of the plastic thereby reducing the risk of collapse during thermal bonding.

There are several other bonding techniques employed to join polymer wafers together: lamination, gluing, laser welding, ultrasonic welding. In lamination, a thin PET foil is coated with adhesive layer. This foil is hot rolled on the wafer containing channel. The adhesive melts and join the lid to the channel wafer. However, it is possible that the adhesive might block the channel after melting. Lid can also be joined to the wafer containing channel with conventional glue. In laser welding, the interface between channel wafer and the lid is locally heated using a laser which is results in a good bond. But the heating procedure is time-consuming process and not recommended for long weld lines. Based on the same principle, ultrasonic welding joins two polymer wafers together by locally heating the interface between the wafers, thus producing good bond.

Ultrasonic bonding requires clean-room processing as particle contamination can adversely affect the bond quality [2].

1.3 Motivation

It is apt to say, "Our world is shrinking". Microtechnologies developed late last century are paving a way to nanotechnologies in the 21st century. Feature sizes are dropping to a few nanometers (billionth of a meter) and technologies to produce such small structures are being developed all over the world. Nanofluidics is a prominent field in this arena. Scientists and researchers have realized the immense potential of nanofluidics in the fields of biology, chemistry, engineering etc. Nanofluidics gives us the ability to observe various phenomena at molecular dimensions. For example, a chemical reaction can be observed in a nanochannel to understand how molecular interactions affect end-products produced, reaction time etc. At the same time, at nanoscale dimensions, number of studies can be performed simultaneously on compact chips thereby considerably improving through-put. Various lab-based pathological procedures can be compacted into a nanofluidic chip to carry out various tests simultaneously in order to reduce the analysis time and cost.

Success of nanotechnology largely depends on the fabrication technology used to produce nanoscale structures. For nanotechnology to benefit the common man, these fabrication technologies should be able to mass-produce nano-devices at affordable cost. Current manufacturing technologies like electron beam lithography, focused-ion beam lithography and other advanced nanolithographic techniques, as explained above, are either very expensive or time-consuming. At this stage, their application to mass-produce nanoscaled devices is out of scope. Thus, there is an extreme need for cost-effective fabrication techniques that can mass-produce nanoscaled devices.

Scientists in the field of nanofluidics are investigating the use of polymers for manufacturing nanofluidic devices. Polymers such polycarbonate, PMMA are being used to fabricate microfluidic devices [15] [24] [28]. Plastics are cheap, bio-compatible and abundantly available. They are easy to machine and their surface properties can be chemically modified. Most of the plastics are optically clear to most wavelengths and are thus compatible with various optical detection and imaging techniques. Plastics can be chemically modified to transmit lights of certain wavelengths. Thermoplastics can be mechanically manipulated for desired effect. Moreover, thermoplastics can be used to mass produce fluidic channel networks with well-developed thermal imprinting and bonding techniques. Thus, polymers are versatile materials that can be effectively employed in modern nano and microfluidic systems and promise to play the same role that silicon played in integrated circuit technology.

1.4 Nanofluidics For Single Molecule Detection

One of the most promising applications of nanofluidics is in detection of individual molecules in fluids. Single molecule detection (SMD) is a methodology to probe a particular individual molecule or sequentially detect an array of individual molecules in a group of molecules. Single molecule detection as apposed to the well-developed ensemble methods like liquid chromatography, electrophoresis, mass-spectrometry provides a more accurate measurement of a parameter under study. In SMD, a study parameter is measured for individual molecule thus providing a distribution of the study parameter for the molecules probed. On the other hand, ensemble methods provide an average value of the study parameter for all the molecules. In analytical chemistry, qualitative as well as quantitative chemical analysis is greatly enhanced by SMD [31]. Moreover, SMD is beneficial in detection of extremely low concentration of target molecules in a high concentration of normal molecules. Sensitivity of ensemble methods is limited and requires much higher concentration of target molecules for efficient detection. This can be extremely crucial in applications such as detection of early-stage cancer when the concentration of tumor markers is extremely low. Detection of early-stage cancer is crucial to success of tumor treatment surgeries [11].

A key requirement for single molecule detection is to limit the number of molecules in the detection volume so as to ensure that all the molecules in the sample can be detected with the probing laser. A way of doing this is by focusing the laser to a small detection volume. However if the detection volume is bigger than the probe volume of the laser, then the molecules outside this probe volume will not be detected, thus

hampering the detection efficiency. Nanochannels, on the other hand, provide physical constriction to restrict the number of molecules in the detection volume and keeping the detection efficiency high at the same time. Nanochannels with detection volumes matching the probe volumes of lasers can be efficiently used to detect individual molecules in a sample. Detection volumes to the order of femtoliter (10^{-15} liter) can be developed in nanochannels. Nanochannels fabricated using top-down or bottom-up approaches can be used for SMD. Moreover, nanofluidic systems require a smaller sample size and have the advantage of faster and accurate analysis when compared to conventional ensemble methods.

Current single molecule detection methods use laser induced fluorescence detection of individual molecules e.g. confocal fluorescence microscopy. When the molecule of interest passes through a laser beam, it gives out a fluorescence burst during its transit through the laser beam, and is detected by an optical detector. The duration of this fluorescence burst depends upon the transit time of the molecule through the beam, the diffusion time of the molecule through the beam and photobleaching time for the molecule. The total number of photons in the photon burst depends upon the spectral properties, the transit time and laser irradiance. Photobleaching limits the number of photons emitted by a molecule. Nanofluidic devices provide effective flow control techniques to optimize the transit time of the molecule through the detection volume for efficient single molecule detection [31].

Chapter 2: Nanochannel Fabrication Concept and Implementation

This chapter presents the idea behind the nanochannel fabrication technique conceived. A finite element, analytical model used to predict the reduction in the microchannel dimensions under the action of applied lateral, compressive strain is presented. An experimental verification is performed on a PDMS microchannel to assess the feasibility of the nanochannel fabrication approach and verify the concept.

2.1 Fabrication Concept

Various nanochannel fabrication techniques were discussed in chapter one. Lithography was a common method employed in these different techniques. The nanochannel fabrication technique pursued here is a non-lithographic approach to fabricate local nanochannel constrictions along microchannels in thermoplastic microfluidic chips.

This technique relies upon local, thermo-mechanical deformation of a section of microchannel in a thermoplastic chip to form a nanoscaled, in-line constriction. Thermoplastics are polymers that can be formed and shaped when heated and can be reformed over and over again with successive heating. This property has been very attractive to researchers and scientists working in the field of polymer micro and nanofluidics, as complex microchannel networks can be replicated into thermoplastics from a single silicon template, thereby considerably reducing the manufacturing cost and time. Some commonly used thermoplastics are polycarbonate and PMMA. The temperature at which thermoplastics become mechanically pliable is called the glass transition temperature (T_g). Glass transition temperature of any material marks the

temperature at which a sudden drop in its elastic modulus is observed. As the temperature of the thermoplastics is increased, their moduli of elasticity decrease making them flexible enough to mechanically deform. This forms the basis of this nanochannel fabrication technique.

A microchannel with a rectangular cross-section is fabricated in a thermoplastic chip, PMMA in this case, with hot embossing and thermal bonding procedures as explained in chapter 3. The cross-sectional dimensions of this microchannel are in the order of few micrometers (< 10 micrometers). The thermoplastic chip containing the microchannel is heated to its glass-transition temperature making it mechanically pliable. The chip can then be mechanically strained in a specific direction to locally deform the microchannel to a nanochannel constriction at the deformation site. Thus, if a local, compressive strain is applied in the direction parallel to the microchannel cross-section, i.e. perpendicular to the length of the channel and thickness of the chip, the microchannel cross-section at the deformation site undergoes maximum in-plane deformation to nanometer dimensions. This local, compressive strain can be applied with the help of thin, rigid plate probes (Fig. 2.1).

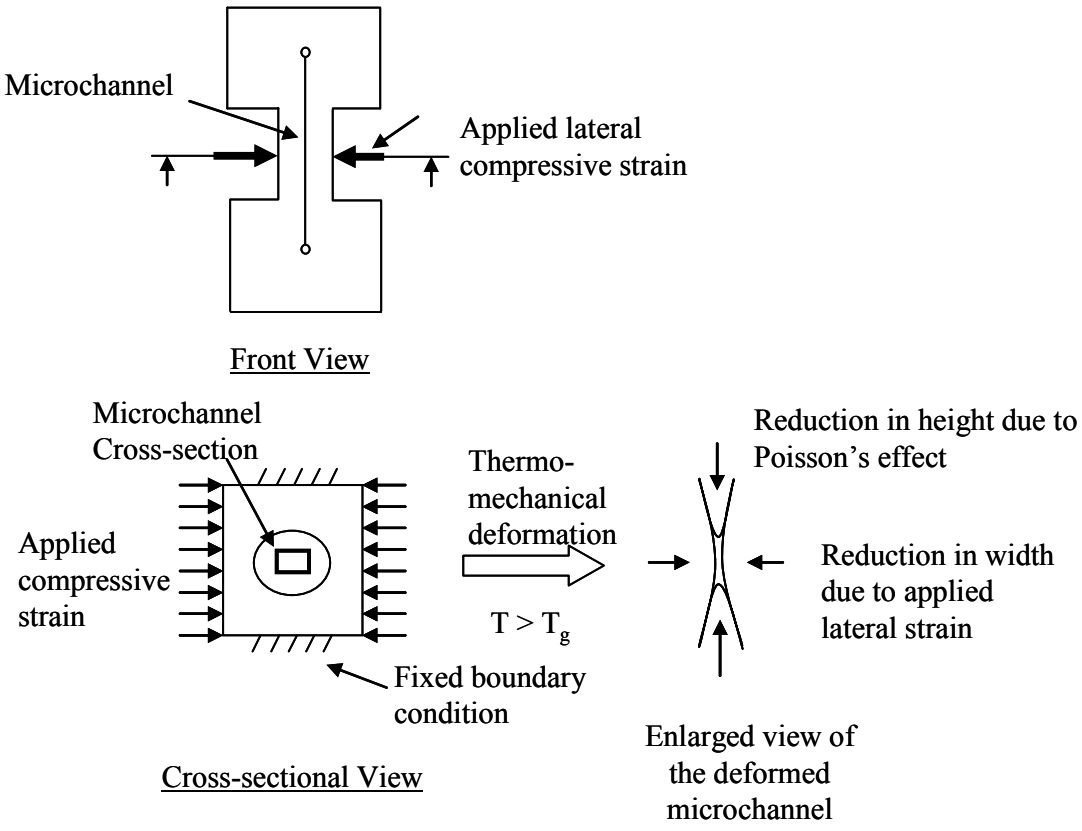

Figure 2.1 Thermo-mechanical nanochannel fabrication concept.

As the lateral, compressive strain is applied on a microchannel, it undergoes deformation in such as way that the width of the channel at its center will undergo maximum reduction, gradually increasing from center to top and bottom of the channel. At the same time, as a result of Poisson's effect, there would be increase in height of the channel. However, if the top and bottom faces of the microchannel chip are mechanically constrained, then the top and bottom sides of the microchannel will undergo a deformation towards the center of the microchannel thereby reducing its height. Thus, under the action of uniaxial, compressive strain, a reduction in two dimensions of the microchannel cross-section can be obtained producing a potential two-dimensional nanochannel. Single molecule detection can be performed at the maximum

deformation location, where the microchannel has undergone maximum deformation. The nanochannel dimensions can be controlled by controlling the applied strain and the deformation temperature.

A similar approach was taken by Sivanesan et al to fabricate a nanoscale channel in a polymer microfluidic chip by thermo-mechanical deformation. Thermoplastic preforms containing microchannels were locally heated to their glass transition temperature and were mechanically pulled along the length of the microchannel. Due to Poisson's effect, the dimensions perpendicular to the direction of applied tensile strain reduced accordingly. Thus, the initial microscaled cross-section reduced to nanoscale at a particular location along the initial microchannel [28]. However, this approach created nanochannels with lengths in the order of few millimeters. In order to pass fluid through these long nanochannels, a high pumping pressure will be required that can potentially cause delamination in the chip or very low flow rates will be required, which might not be attractive for applications requiring variation of flow rate like single molecule analysis.

Similarly, Sundararajan et al have used lateral compressive strain to deform single layer PDMS membranes for microfluidics peristaltic pumping, microfluidics cell sorting and micro-mixing applications [30].

2.2 Proof of Concept

A plain strain, finite element model was developed using ANSYS® to understand the deformation behavior of a microchannel under the action of applied lateral, compressive strain. Effects of variation in the initial cross-section of the

microchannel, i.e. cross-section of the microchannel when no strain is applied, on the final cross section of the deformed microchannel were also studied. Experimental validation of the phenomenon was performed by mechanical deformation of a PDMS microchannel. PDMS is a rubber-like elastomer, which can be deformed easily.

2.2.1 Finite Element Model

A finite element model developed in ANSYS® was used to study the variation in height and width of a microchannel with applied lateral compressive strain and the effect of initial aspect ratio of the un-deformed channel on deformation dynamics. 2D, 8-node, plain strain elements were used for this structural analysis. Since the cross-section of the channel is symmetric about its vertical and horizontal axes, symmetric boundary conditions were applied and only a quadrilateral of the cross-section was used for analysis. Fixed boundary conditions, as explained in preceding sub-chapter, were not applied in the model for deformation of PDMS microchannel, as the primary investigation objective was to understand the reduction in width of the channel along its height with the applied strain and theoretically verify the concept. Increase in the height of the microchannel was also estimated with this model. It was after the investigation of deformation dynamics of PDMS microchannel using this model that the need for fixed boundary conditions was realized and incorporated in the fabrication approach as explained further in this section. The model was modified to incorporate the fixed boundary conditions to study the deformation in thermoplastic microchannel chips. Linear, elastic, isotropic material properties are assumed for simplicity.

The model approach was based on varying the shape of a microchannel in PDMS to understand the reduction in widths of the channel at its center and top/bottom

under the applied compressive strain. For a constant microchannel width (5 μm), the height of the microchannel was varied from 1 μm to 10 μm. The applied lateral, compressive strain is increased to a value, where the final minimum channel width reduces to 1 μm and 0.5 μm. This is performed for all 10 cases, i.e. height varying from 1 μm to 10 μm with constant width of 5 μm. The deformation behavior was also studied for microchannel with 10 μm width.

2.2.2 Model Results

Figure 2.2 shows the nomenclature used for the heights and widths of the microchannel at different locations. Variation of the width at the channel center, indicated by 'a' and top/bottom, indicated by 'b', with the applied strain was studied along with the variation in the height of the channel at its center (c). The height of the side-walls was indicated by 'd'.

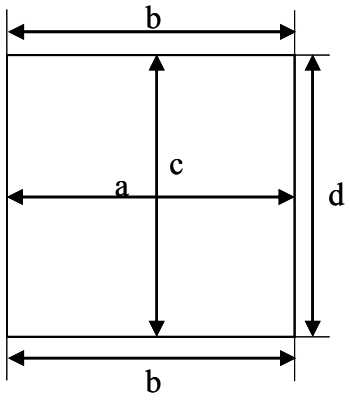

Figure 2.2 Microchannel cross-section dimensioning nomenclature.

a - Width at the center of the channel (micrometers)
b - Width at the top of the channel (micrometers)
c - Height at the center of the channel (micrometers)
d - Height of the side walls of the channel (micrometers)

This dimensioning nomenclature was used in the model results plots for simplification. Note that these are microchannel dimensions and not the dimensions of the cross-section of the plastic chip containing the microchannel.

The model results indicated that the deformation in the width (a) at the center of the channel is higher than the widths (b) at top and bottom of the channel, irrespective of the strain applied and the initial cross-section of the microchannel. The difference between the width at the center and top of the channel increased as the applied strain was increased, indicated by the reduction in ratio of the widths at the center of the channel and at the top of the channel from 1 (no strain applied case, when the side walls of the channel are perfectly vertical) to very close to zero (Fig. 2.3). This means that the channel gets narrower at its center than at top and bottom as the strain is increased. In case of shorter channels, i.e. height (c) less than width (5 μm), for lower applied strain values, the rate of decrease of widths at center and the top/bottom of the channel was almost similar indicated by shallow slope of the plot lines. However, for higher strain values, the width at the center of the channel reduced rapidly than at the top/bottom of the channel. On the other hand, for taller channels the rate of decrease in the width at the center of the channel was higher than at the top/bottom of the channel for all values of applied strain as indicated by the higher slopes of the plot lines for all strain values (Fig. 2.3). For final deformed width of 1 μm at channel center, the ratio of widths at center and top/bottom (a/b) decreased as the initial aspect ratio (height:width) increased. Thus, for taller channels (aspect ratio > 1) when the width at the channel center reduces to sub-micrometer dimensions, the widths at top and bottom are well above a micrometer.

On the other hand, under the action of the applied strain, the height (c) of the channel at its center increased as indicated by the increasing slopes of the lines in Fig.2.4. Moreover, for taller microchannels, the increase in height of the channel at its center after deformation was higher than for shorter microchannels for the same final deformed width at the channel center (a_final = 1 μm).

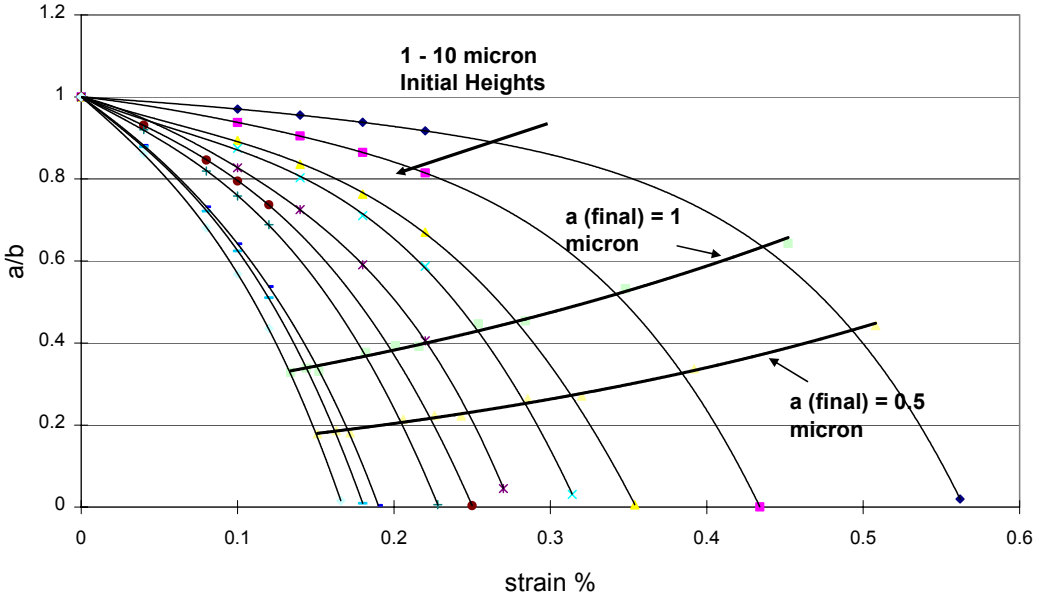

Figure 2.3 Reduction in widths of the microchannel at center and top/bottom with applied strain.

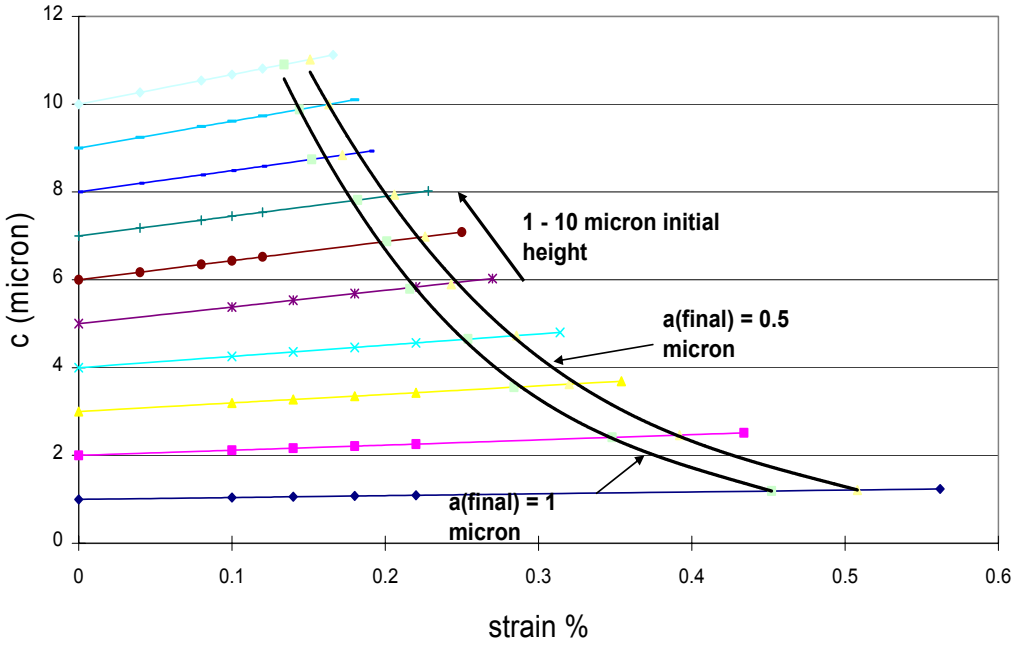

Figure 2.4 Increase in height of the channel at its center with applied strain.

The model results indicated that under the action of lateral compressive strain, the rectangular cross-section of the microchannel undergoes a deformation to an hour-glass shaped outline with only some part of the cross-section in sub-micrometer region. Thus, it was imperative to reduce the difference in widths at the center and top/bottom of the deformed microchannel to get a consistent sub-micrometer channel dimensions. This was achieved by applying fixed boundary conditions on top and bottom faces of the microchannel chip during the thermo-mechanical deformation process. The top and bottom faces of the microchannel chip are the faces of the thermoplastic chip parallel to the microchannel length and perpendicular to the chip thickness. This fixed boundary condition would force the top and bottom horizontal sides of the microchannel cross-section to bend towards the channel center, thereby reducing its height. Thus, during the deformation procedure, the rectangular cross-section of the microchannel will reduce in all directions. As a result, the initial longer curvature of the microchannel

sidewalls after deformation is replaced by just a small section of that curvature thereby keeping the width of the deformed microchannel below micrometer along its height (Fig. 2.1).

This finite element model was further modified to incorporate the fixed boundary conditions on the faces of the microchannel chip. Here, a microchannel in PMMA is considered with the actual cross-section of the chip used in the development process. The channel is 10 μm wide and 5 μm high. Lateral, compressive strain is applied to deform the width of the channel at its center to 1 μm and 0.5 μm. It was observed from the model results that due to the fixed boundary conditions, the top and bottom sides of the channel bend towards the center of the channel.

As a result of incorporation of fixed boundary conditions in the model, when the width at the center of the channel reduced to 1 μm from 10 micrometers, the height of the channel at its center reduced to 1.32 μm from 5 micrometers. At the same time, when the width at the channel center reduced to 0.5 μm, height of the channel at its center reduced to 0.76 μm from 5 micrometers. Thus potentially, a one-dimensional nanochannel can be obtained with inclusion of fixed boundary conditions during the thermo-mechanical deformation.

2.2.3 Experimental Validation

The purpose of experimental validation was to quickly verify the trend in deformation of the channel width and height under the action of applied strain. A compressive, lateral strain was applied on a square microchannel (5 μm x 5 μm) in PDMS. The microchannel was prepared in PDMS by soft lithography methods as explained in chapter 1. SU8, a negative photoresist was patterned on a silicon wafer with

a native oxide layer to form a master template for soft lithography. PDMS is poured on the template to form a 0.5 mm thick layer. The volume of the PDMS can be adjusted so as to form an approximately 0.5 mm thick layer. The PDMS layer was then peeled-off from the template with imprinted channels and was capped with another flat, 0.5 mm thick PDMS layer to form an enclosed microchannel.

The PDMS enclosed microchannel was cut using a 200 μm thick blade in such as way that the width of the PDMS enclosure was approximately 1 mm. Thus, the cross-section of PDMS enclosure was around 1 mm x 1 mm, with microchannel roughly at its center. A compressive, lateral strain was applied with two identical mechanical micrometer linear stages from Newport Corporation[†]. The cut PDMS microchannel was placed between two flat plastic plates attached firmly to the linear stages. A specific strain can be applied to the microchannel by providing precision displacement using the micrometer linear stages. The deformation in the cross-section is observed under an optical microscope (Fig. 2.5).

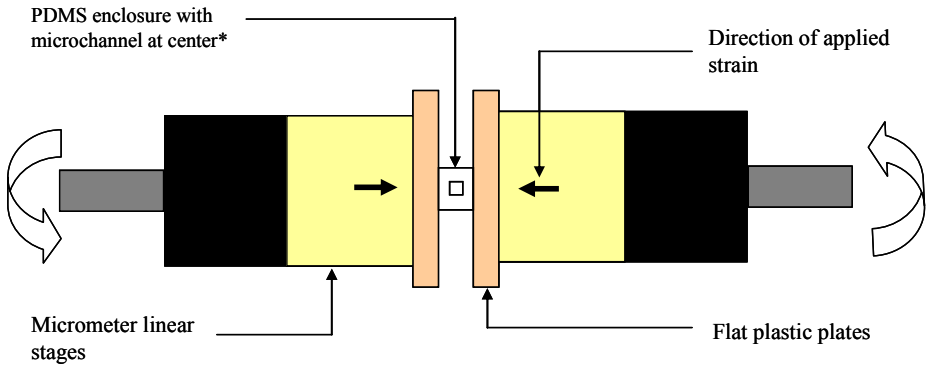

Top View (Direction of optical measurement)

* Not to scale

Figure 2.5 Experimental setup for PDMS microchannel deformation.

[†] Newport 460A Series High Performance Integrated Ball Bearing Linear Stages. URL: www.newport.com

The experimental data indicated a similar trend in the microchannel width and height variation with the applied strain (Fig. 2.6, Fig. 2.7). The differences in the experimental and model data can be attributed to the model assumptions along with several manual and experimental limitations.

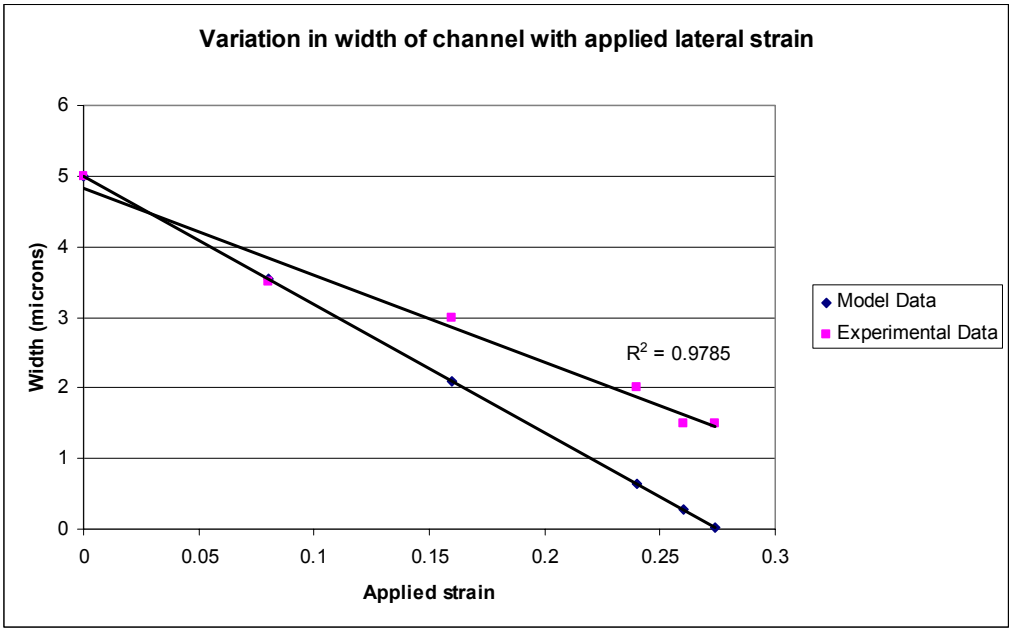

Figure 2.6 Reduction in width of microchannel in PDMS with applied lateral, compressive strain.

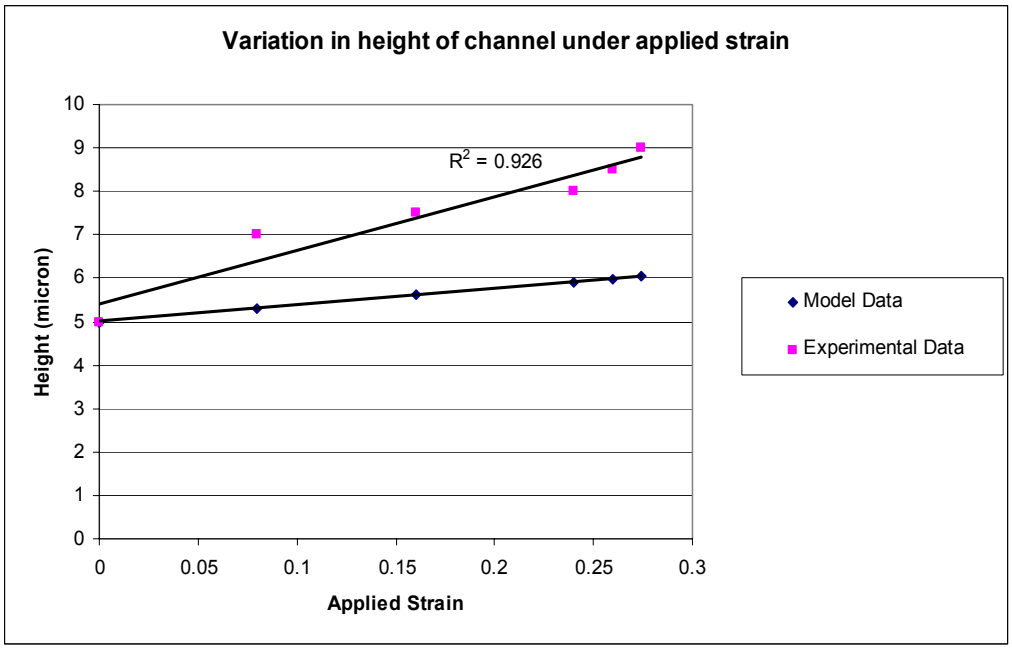

Figure 2.7 Increase in height of the microchannel in PDMS with applied lateral, compressive strain.

A plane strain analysis was assumed for the finite element model developed. The underlying assumption for a plane strain analysis is that the strain in the direction perpendicular to the deformation plane is negligible. Hence in this case, the strain in the direction of the observation (i.e. perpendicular to the PDMS cross-section being observed) should be negligible as compared to the strain in plane of deformation. However, since the observed cross-section was a free-surface, the strain in the direction perpendicular to the free surface, i.e. perpendicular to the applied strain's plane was considerably high. This contributed to the discrepancy between the plane strain model results and experimental data.

There were fabrication limitations in precisely cutting the PDMS enclosure to get the microchannel exactly at its center. Any deviation in the microchannel position from the center of the PDMS cut-out will lead to asymmetry causing unexpected

deformation dynamics. The cross-section of the PDMS enclosure formed a bulge in the direction of observation due to the Poisson's effect of the applied lateral, compressive strain. Thus at higher magnification optical detection, the whole microchannel cross-section was not in a single plane of focus, as a result of which a blurred image of the deformed channel was observed. It thus became hard to measure the deformed channel dimensions. This aggravated at higher applied strains. The measurements were further worsened by external noise such as vibration.

2.3 Thermo-mechanical Deformation Approaches

Various thermo-mechanical deformation approaches to produce a pre-determined, lateral compressive strain were evaluated. These approaches were primarily based on the mode of microchannel chip-heating employed and the strain application method. One dimensional heat conduction and convective heating were the two chip-heating methods employed. Lateral and vertical strain applications were the two strain application modes considered. Lateral and vertical strains imply the direction of the strain applied with respect to the chip plane (See section 2.2.1 for chip plane). The initial microchannel dimensions used were 100 μm x 50 μm (width x height). Such bigger microchannels were used to first check the feasibility of the approaches under consideration to provide controlled, thermo-mechanical deformation to produce nanochannels.

2.3.1 Approach 1: One dimensional conductive heating and lateral compressive strain application.

In this method, the plastic chip was placed on a highly polished, ceramic heating plate. The heating surface of the plate was set to a temperature just above glass-transition temperature of the plastic. Polycarbonate chips were used in this case with glass transition between 145^{o}C and 150^{o}C. The surface of the heating plate was set at 160^{o}C. A polished steel plate was placed on top of the plastic chip so as to keep uniform thermal boundary conditions on top and bottom of the chip as the chip heats up. Since steel has high heat capacity, it will reach a temperature close to the heating temperature. A thermocouple was attached to the plastic chip at the steel plate interface. The chip was heated until the thermocouple displayed a constant steady state temperature. The red arrow indicates the direction of heat flow. An aluminum plate attached to a micrometer linear stage was used as probe to produce lateral strain on the chip (Fig. 2.8). The faces of this aluminum probe were polished so as to provide uniform strain perpendicular to the channel length. However, it was observed that the temperature varied considerably across thickness of the plastic chip. A temperature difference of about 20^{o}C was observed between the heating surface and top of the plastic chip. Thus the modulus of elasticity will vary across the plastic chip, which will affect the deformation dynamics and therefore this approach was not further pursued.

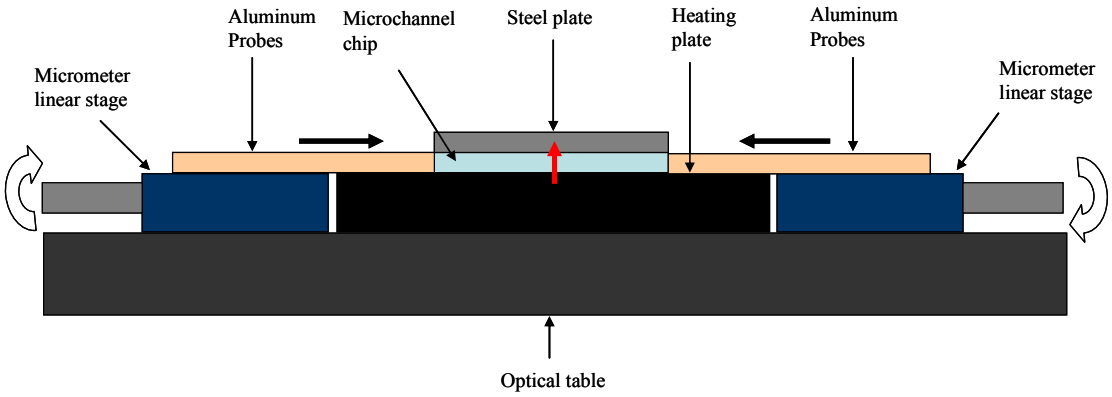

Figure 2.8 Experimental setup of conductive microchannel chip heating and lateral strain application.

2.3.2 Approach 2: Combined conductive and convective chip heating and lateral compressive strain application.

It this approach, the plastic chip with the micro-channel at its center was placed on a polished ceramic heating plate set at a temperature just above the glass transition temperature for the plastic. A heating gun was placed vertically above the chip. The heating gun was set to a temperature so that the temperature of the hot air at the chip top surface was close to hot plate temperature (Fig. 2.9). The lateral strain was provided by polished aluminum plates attached to mechanical micrometer linear stages similar to the previous approach. This arrangement was used to ensure similar thermal boundary conditions on top and bottom of the chip. However, it was observed that the plastic chip temperature was considerably less than the heating plate temperature (around 20^{o}C temperature difference was observed). This can be attributed to the thermal resistance between the plastic chip and the heating plate and also the thermal resistance provided by the chip itself. The thermal conductivity of the plastics is very low, which results in higher thermal resistance. The temperature distribution on top of the chip is not uniform

as the temperature in a plane from the heating gun tip is not uniform, which resulted in non-uniform heating of the top surface of the chip. Thus, the temperature of the chip remained below the glass transition temperature and the chip could not be deformed using this setup. The heating plate was set 40^{o}C and 60^{o}C above the glass transition temperature of the plastic to increase the temperature of the microchannel chip, however bubbles of trapped hot air from the heating gun were observed in the top part of the chip. Due to theses problems, this approach was not used for the required thermo-mechanical deformation.

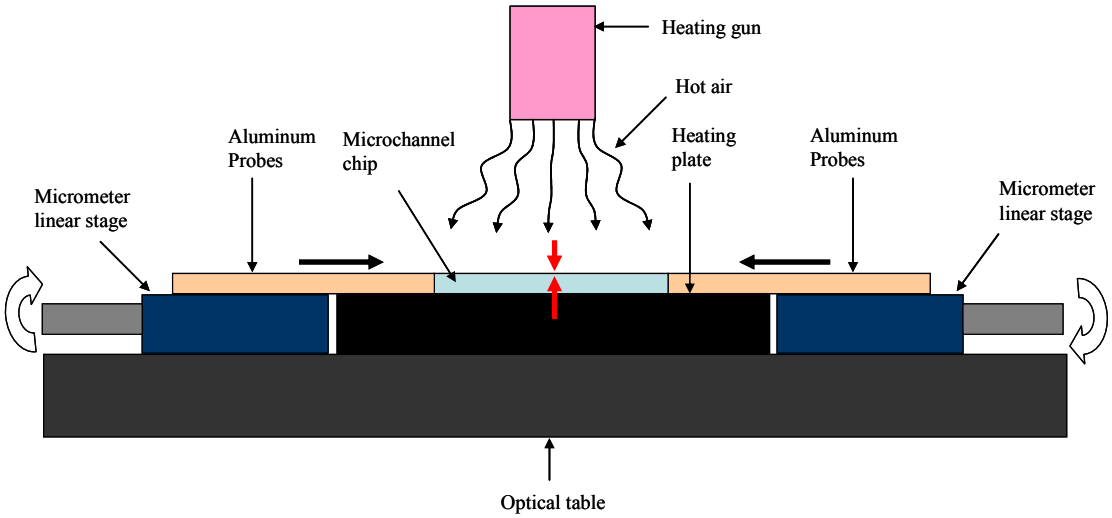

Figure 2.9 Experimental setup of combined microchannel chip heating and lateral strain application.

2.3.3 Approach 3: One-dimensional heat conduction and vertical strain application.

The purpose of this approach was to check the application of Poisson's effect to laterally compress the microchannel to nanoscale by applying vertical strain. In this approach, the microchannel chip was placed on a polished heating plate. Two vertical, plate probes placed on either side of microchannel were used to provide the

vertical strain. 400 μm thick and 5 mm wide aluminum plate probes attached to a mechanical micrometer actuator were used for this purpose (Fig. 2.10). The distance between the probes was varied from 1 mm to 5 mm in steps of 2 mm. For a 3 mm thick chip, vertical displacements from 200 μm to 1000 μm in steps of 200 μm were applied with the probes mounted on vertical, linear micrometer stages. It was observed that the channel collapsed before reducing into the submicrometer dimensional regime. Since one dimensional conduction was used, the temperature of the chip at the top of the chip was about 60^{o}C less that the heating plate surface temperature. This can be attributed to the thermal resistance provided by the gap between the plastic chip and the heating surface and thermal resistance along the thickness of the chip. As a result, a much higher temperature was required to be set so as to make sure that the temperature on top surface of the chip is above the glass-transition temperature for the plastic deformation. Thus the modulus of elasticity of the chip increases from the bottom to the top surface. The chip was thus softer at its bottom surface, which was in direct contact with the heating plate and relatively harder at its top surface, where a vertical strain was applied. Thus, as the applied strain increased, the chip being softer at its center, where the microchannel is located, collapsed the channel completely.

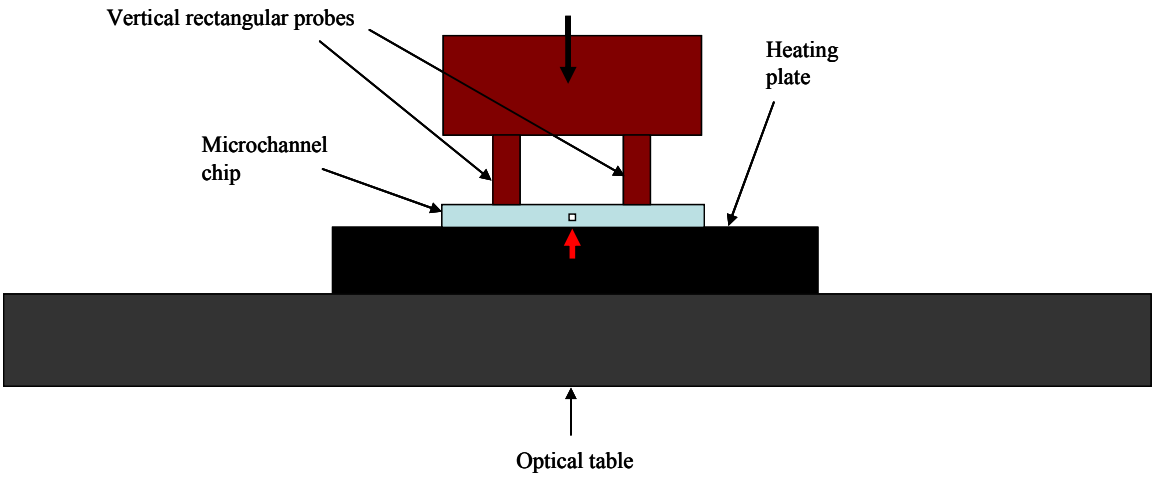

Figure 2.10 Experimental setup of one-dimensional conductive heating and vertical strain

It was concluded from the above-described approaches that uniform heating of the microchannel chip was crucial to ensure proper deformation dynamics under the action of controlled lateral compressive strain. This will in-turn determine the nature of the nanochannel formed. Heating the chip in a convection oven would provide a more uniform heating of the chip. This lead to the design of a compact, custom, mechanical rig that can fulfill the above requirements.

2.4 Final Implementation

A custom, mechanical rig was designed, developed and optimized to thermo-mechanically deform the thermoplastic chip in order to obtain local nanochannel constriction in the microchannel. The two main functions of this mechanical rig are: hold the chip vertical with the channel perpendicular to the deformation probes and provide a pre-determined, lateral, compressive strain to the microchannel chip. The rig is compact enough to be placed in a desktop convection oven (Fig. 2.11).

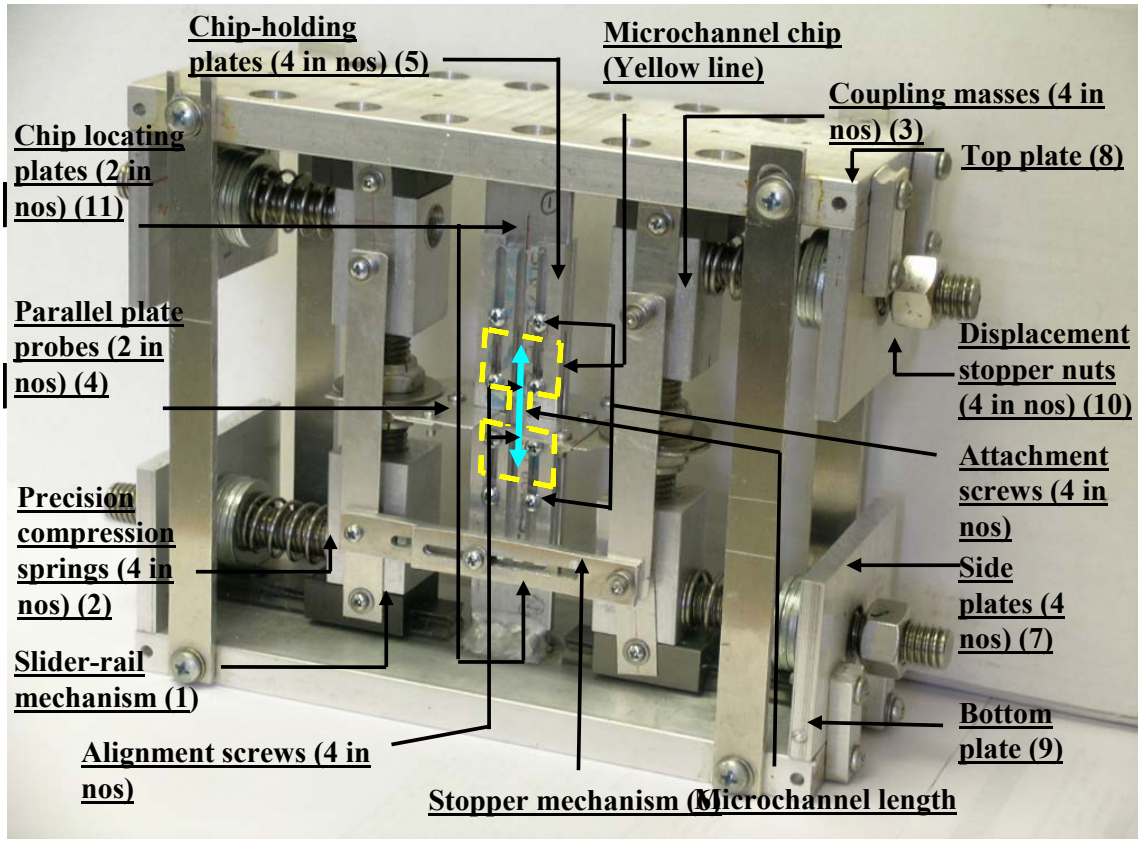

Figure 2.11 Custom mechanical rig for thermo-mechanical deformation of the microchannel chip.

The mechanical rig is an all-aluminum assembly with stainless-steel, precision, compression springs to provide the required strain in the thermoplastic microchannel chip. As can be seen from the figure 2.11, the rig is symmetric about its horizontal and vertical axes with the microchannel chip held at its center (indicated by yellow dotted line). The microchannel is oriented vertically at the chip center as shown by the blue arrow.

The main parts of the rig are slider-rail mechanism (1), precision compression springs (2), coupling masses (3), parallel plate probes (4), chip holding plates (5), stopper mechanism (6), side plates (7), top and bottom plates (8,9), displacement stopper nuts (10) and the chip locating plates (11) (Fig. 2.11). The microchannel chip is held vertically between the two chip-locating plates using four chip holding plates with alignment and attachment screws. The chip locating plates are two, $1/8^{th}$ inch (3.175 mm) thick aluminum plates precision welded to the top and bottom plates, so that they are perpendicular to the top and bottom plates. These chip holding plates have slots, which provide openings for alignment and attachment screws to hold the chip between the chip-locating plates. The slots also provide degree of freedom along its length, which is essential for chip mounting process. The alignment screws ensure that the microchannel in the plastic chip is perpendicular to the plate probes. A diameter clearance of 0.5 mm is provided between the alignment holes drilled in the microchannel chip and the alignment screws to compensate for manufacturing and alignment tolerances. The chip holding plates are screwed to the chip locating plates with the microchannel chip sandwiched between the chip-holding plates. The alignment screws along with the chip holding plates prevent any motion of the chip relative to the plate

probes during the indentation process. The chip-holding plates also ensure that the plate probes move in one plane during the deformation process, thereby eliminating/reducing any offset in co-linearity of the plates. The coupling masses attached to the slider mechanism transfer the expansion of the compression springs to the aluminum plate probes through horizontal and vertical threaded rods that results in lateral compressive strain on the vertically held chip. The slider is made out of ceramic-lined aluminum and slides over an aluminum rail. Thermal grease is applied between the slider and rail to reduce friction effects due to thermal expansion while operating at deformation temperature (~120^{o}C). Symmetric arrangement of the compression springs eliminates bending in the probes. Precision compression springs pass over horizontal, 0.5 inch threaded rods (1/2"-13[†]) connected to the coupling mass. These threaded rods pass through clearance holes in the sides plates, which are attached firmly to the base and top plates. A similar assembly is made on the top plate and the coupling masses on these assemblies are connected together through vertical, 0.5 inch threaded rods (1/2"-13). The parallel plate probes are held firmly between two lock nuts on these threaded rods. This arrangement provides position adjustment of the probes along the threaded rods for their in-plane alignment. The top and bottom plates are connected together with four, 1/8th inch aluminum plates. Nuts placed on the horizontal rods are used as displacement stopping devices. Thus, these nuts can be placed at a distance from the side plates that will decide the extent of compressed spring expansion and thereby the compressive strain applied to the chip. The distance between the stopper nuts and the side plates can be decided by the number of revolution of the nuts over the threaded rod (1 revolution = 1.96 mm or 2 mm approximately). The stopper mechanism consists of a tightening screw and nut assembly

[†] ½"- 13 indicates ½ inch diameter threaded rod with 13 threads per inch.

passing through two slotted aluminum plates. The friction between the tightened screws and the aluminum plates prevents the compressed springs from expanding until the screw is loosened. The stopper mechanism ensures that no indentation is produced on the chip until the rig and the chip reach a steady-state thermal condition. Once the assembly reaches preset temperature in the convection oven, the screw can be manually loosened to initiate the expansion in the compressive springs thereby providing gradual, lateral, compressive strain on the microchannel chip.

Chapter 3: Nanochannel Fabrication Process

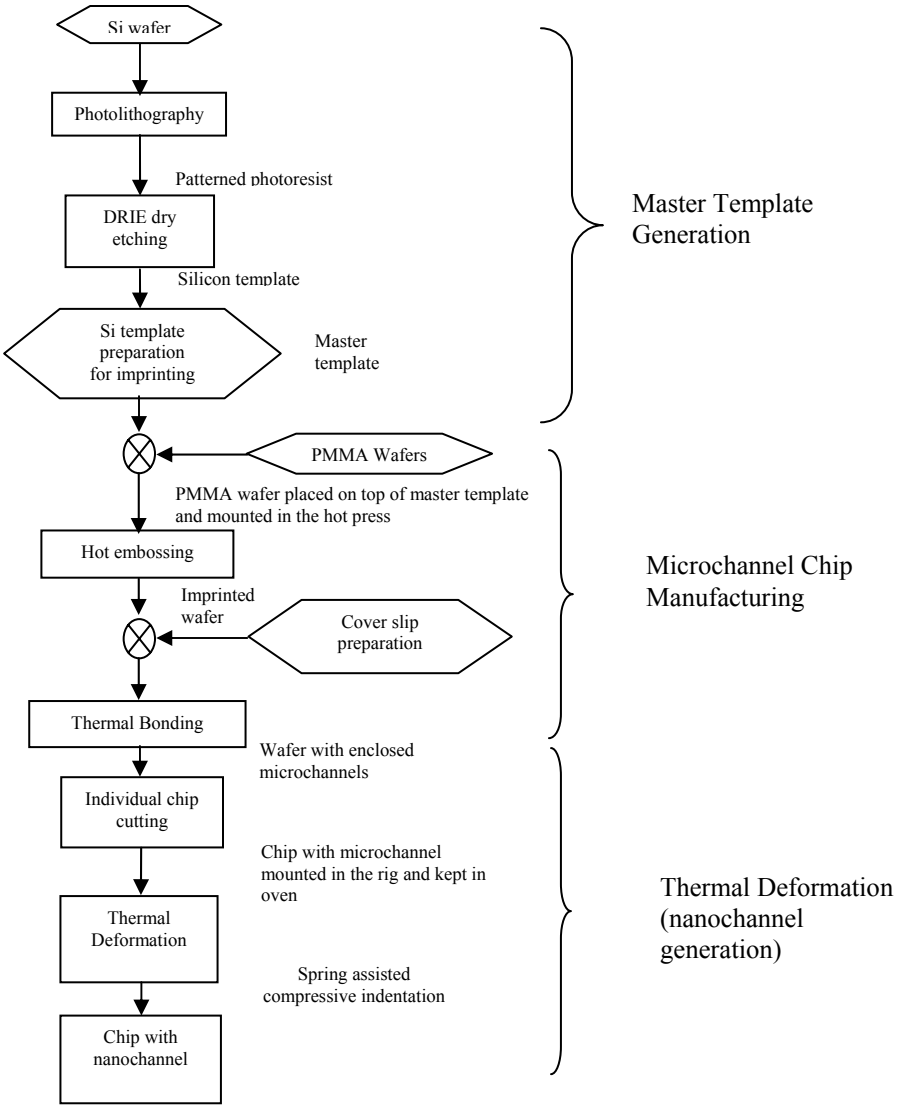

Figure 3.1 Fabrication process flow in nanochannel development

The nanochannel fabrication process developed can be divided into three major steps: master template generation, microchannel chip manufacturing and thermo-mechanical deformation of the microchannel to nanoscale (Fig. 3.1). Fig. 3.1 shows the nanochannel fabrication process flow. A <100> silicon wafer was used to generate the master template with standard photolithography and deep reactive ion etching (DRIE). A

PMMA chip containing the microchannel was generated from Si master template, developed in step 1, with hot embossing and thermal bonding techniques. Final chip with nanochannel constriction was developed by directed mechanical deformation of the heated microchannel polymer chip, using the custom mechanical deformation rig. The nanochannel chip can further be post-processed (milling and mechanical polishing) for application in optical detection of single molecules.

3.1 Master Template Generation

Master template generation consists of two steps: photolithography and deep reactive ion etching (DRIE). In the first step, a photoresist pattern was developed on the Si wafer surface, which was further used as a mask for DRIE. DRIE dry etching further transfers the topographical photoresist pattern to the Si wafer, creating rectangular structure on the wafers surface. The structures on etched Si wafers were further hot embossed on PMMA wafers. The pattern consists of microchannels, 25 mm long and widths varying from 5 micrometers to 25 micrometers.

3.1.1 Photolithography

A 4 inch, virgin <100> Si wafer was rinsed in solvents (Acetone, Methanol and IPA) to clean its surface and baked over-night at 120^{o}C. Baking ensures proper removal of moisture from the substrate's surface, which results in better adhesion for the photoresist on the wafer surface. AZ® 9245[†], a positive photoresist was used for photolithography.

[†] AZ® 9245 is a thick film positive photoresist from Clariant Corporation, Somerville, New Jersey, USA. URL: www.azresist.com

The silicon wafer was vacuum held on a wafer-chuck in SCS G3P-8[††] spincoater. Few drops of Hexamethyldisilazane (HMDS) were put on the wafer surface and allowed to stand for 3 minutes. HMDS is then spin-coated at 4000 rpm for 30 seconds to form a thin layer on the wafer surface. HMDS was used to enhance the adhesion between the wafer surface and the coated photoresist. The positive photoresist, AZ® 9245 was spin coated on the surface of the wafer to form a 4.5 μm thick layer. The spinning was done at 3000 rpm for 30 seconds. The resist coated wafer was pre-baked at 90^{o}C for 2 minutes to remove any excess moisture. The pre-baked wafer was exposed to UV light (wavelength ~ 250 nm) for 150 seconds at a dose of 6.5 mW using Karl Suss MA6 Mask Aligner[‡‡]. A soda-lime, chrome mask is used in this step. To achieve fine channel widths to the order of 5 μm, film mask cannot be used. The exposed wafer was post-baked at 90^{o}C for 2 minutes to enhance adhesion between the unexposed resist and the wafer.

The exposed wafer was developed in AZ® 400K[‡] developer solution for about 3 minutes. A combination of immersion and spray development techniques was used to make sure that narrow structures do not delaminate from the wafer surface. It was observed that only immersion development delaminated 5 micrometer wide structures from the wafer surface.

The Si wafer was dry etched using deep reactive ion etching machine. The wafer was exposed to give required etch depth. One cycle of DRIE was composed of 10

[††] SCS G3P-8 is a programmable spin-coater produced by Speciality Coating Systems, USA. URL: http://www.scscoatings.com/index.cfm

[‡] AZ® 400K is a developer solution for AZ® series positive photoresists distributed by AZ electronic components USA corporation.

[‡‡] Karl Suss MA6 mask aligners uses contact lithography to produce fine photoresist structures as small as 2 μm.

seconds of etching and 6.5 seconds of passivation step. 14 cycles gave an etch depth of 5 µm and 9 cycles gave an etch depth of 3 µm. DRIE gives vertical side-walls, which are crucial for the nanochannel development process. Before etching, the wafer with photoresist pattern was treated with oxygen plasma for 8 seconds.

After DRIE, the photoresist was stripped-off from the wafer surface by immersing in Nanostrip®[†] for 2 hours at 60°C. The Si wafer was then used as a master template for hot-embossing its pattern on thermoplastic (PMMA) wafers (Fig. 3.2).

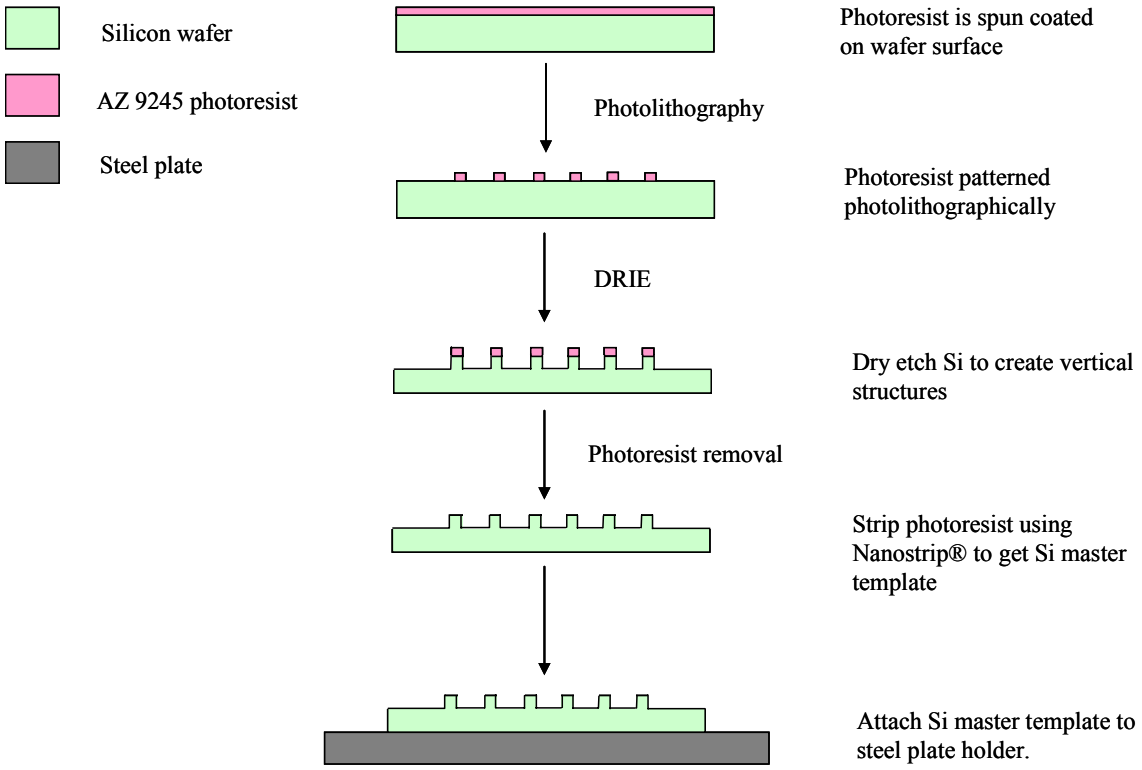

Figure 3.2 Fabrication process flow for lithography

[†] Nanostrip® is a stabilized piranha solution produced by Cyantek Corporation, Fremont, California USA. URL: http://www.cyantek.com/. Note that Nanostrip is extremely corrosive and should be handled carefully. Refer MSDS before use.

3.1.2 Template preparation

The developed Si wafer was attached to a smooth steel plate using Pyralux®[†] LF adhesive sheet (Fig. 3.2). This attached wafer was further used in Carver Hot Press for hot embossing PMMA wafers.

The Si wafer was placed on a 1/8th inch (3 mm) polished steel plate ((6 inch x 6 inch) or (153 mm x 153 mm)) with the Pyralux® sheet in between. A 0.5 inch (6.35 mm) thick glass plate ((5 inch x 5 inch) or (127 mm x 127mm)) was placed on top of the Si wafer with a Teflon sheet in-between. The Teflon sheet prevents any minute relative lateral motion of the platen of the hot press with respect to the sandwiched layers from transferring to the silicon template while opening the platens, which can shear-off the structures on the Si template (Fig. 3.3).

The sandwich was placed between two hot platens of the Carver Auto Four/15 Hot Press. The platens were set at 170^{o}C. A pressure of 238 psi (1641 kPa) was applied on the sandwiched assembly for 3 hours. The Si template sticks to the bottom steel plate and can be further used for hot embossing polymer wafers.

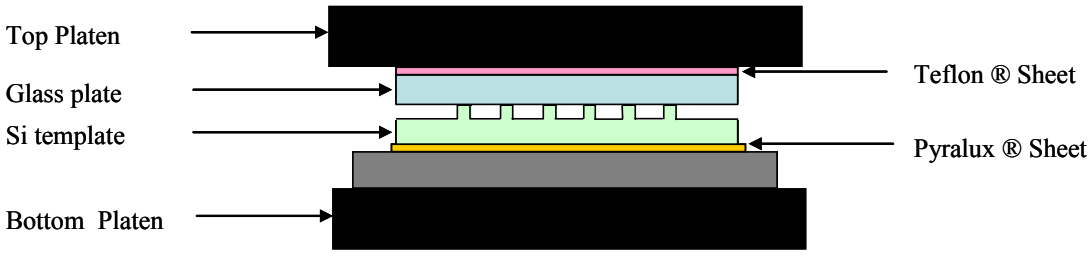

Figure 3.3 Assembly for template preparation.

[†] Pryalux® is a product of DuPont^{TM}. URL: http://www2.dupont.com/Pyralux/en_US/index.html

3.2 Microchannel Chip Manufacturing

This step consists of hot embossing the Si template pattern into a PMMA wafer followed by thermal bonding of a PMMA cover slip with inlet and waste reservoirs to the embossed wafer. This is done in a Carver Auto Four/15 Hot Press.

3.2.1 Hot Embossing

The master Si template was mounted on lower platen of the hot press with the help of a template holder. Make sure that the template is firmly held on the platen so that there is no relative motion of the template with respect to the platens, which can damage the template or imprinted pattern. Tightening screws were used to ensure this.

A 4 inch, 1.5 mm thick PMMA wafer was placed on the master Si template. The PMMA wafer was degassed in a heated (80^{o}C) vacuum oven overnight. A glass plate (same dimensions as explained above) was kept on the PMMA wafer with a Teflon sheet in-between them, forming a sandwich layer of Si template, PMMA wafer, Teflon sheet and glass, bottom to up respectively. A Teflon sheet separates the glass plate from the top platen. The platens' temperature was set to 145^{o}C. A pressure of 100 psi (690 kPa) was applied to the arranged PMMA - Si template sandwich for 20 minutes. The dwell time ensures complete heat transfer to the PMMA wafer for proper reflow of the material resulting in proper pattern transfer. The assembly was cooled down to a temperature just above the glass transition temperature for PMMA (105^{o}C) and the applied pressure was removed. (If the pressure is removed at a temperature lower that the glass transition temperature of PMMA, then silicon from the template sticks to the

PMMA wafer and gets removed from the template surface during demolding of the PMMA wafer). The assembly was then further cooled to 85°C. The imprinted PMMA wafer was demolded with the pattern transferred from the template (Fig. 3.4).

The imprinted side of the imprinted wafer was covered with a blue tack tape† to prevent any dust particles from clogging the channel.

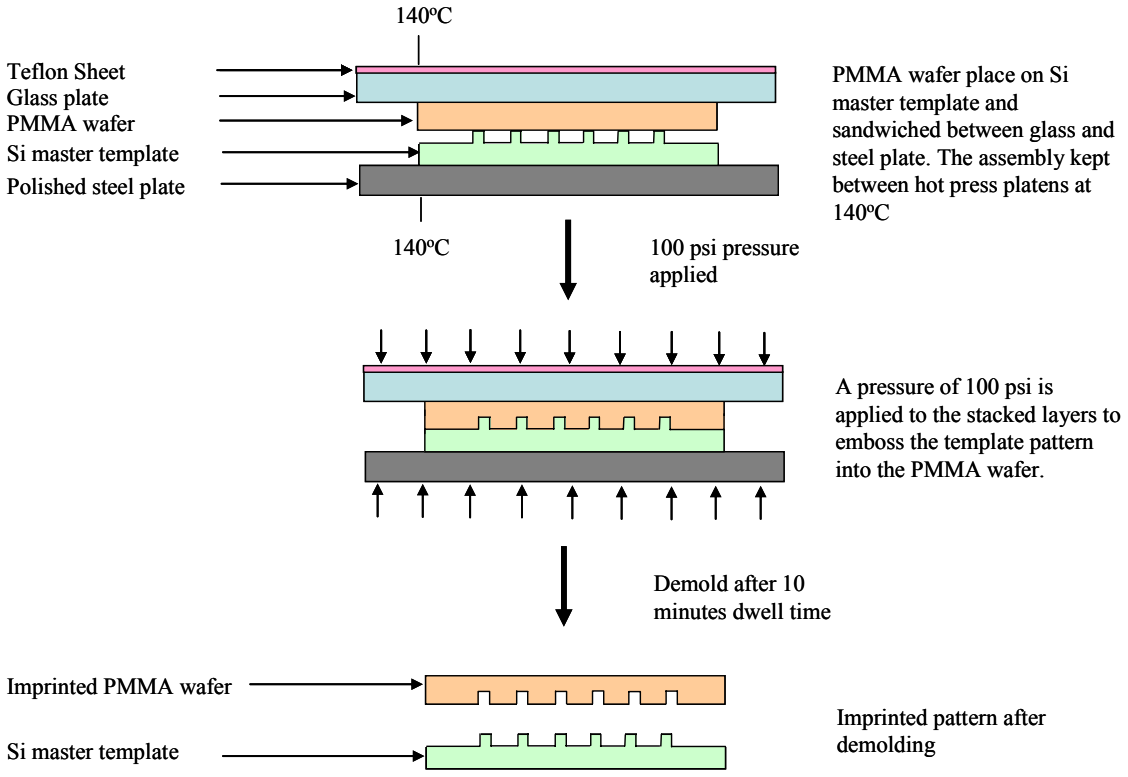

Figure 3.4 Fabrication process flow for hot embossing PMMA wafer.

† The blue tack tape is obtained from Semiconductor Equipment Corporation. URL: www.semicorp.com

3.2.2 Thermal Bonding

Input and waste reservoir holes were drilled in the PMMA cover plate (A cover plate is a 4 inch in diameter, 1.5 mm thick PMMA wafer that is thermally bonded to the imprinted wafer to form an enclosed microchannel). The holes were drilled at locations such that they aligned with the imprinted channels on the embossed PMMA wafer, when the two wafers are put together. The drilled holes were deburred to prevent any clogging of the channel near the reservoirs after bonding.

The PMMA cover plate was placed on the imprinted PMMA wafer so that the drilled holes aligned with the corresponding imprinted channels. These two wafers were then sandwiched between two glass plates. The whole assembly was placed between the platens of the Carver hot press, which were set at 95°C (Fig. 3.5).

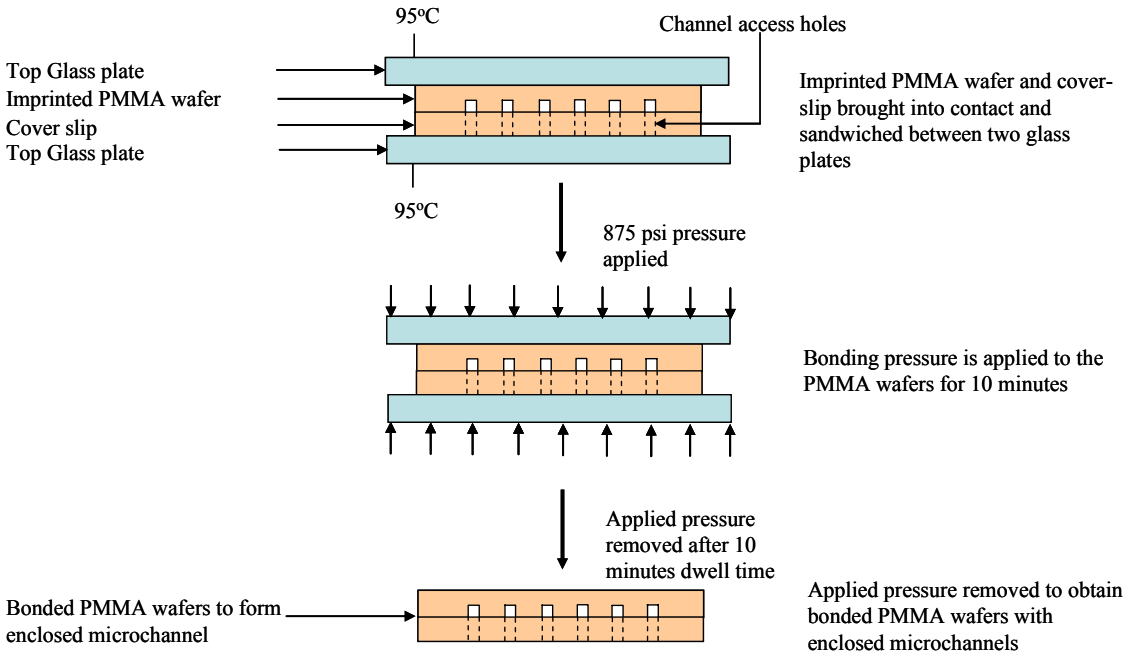

Figure 3.5 Fabrication process flow for thermally bonded PMMA wafers.

A pressure of 1200 psi (8273.7 kPa) was gradually applied to the sandwiched PMMA wafers with increasing platen temperature. The pressure was maintained on the assembly for 15 minutes to ensure complete heat transfer to the sandwiched PMMA wafers for proper bonding (Fig. 3.5).

The applied pressure was removed and the bonded PMMA wafers were allowed to gradually cool down. If the wafers are cooled down rapidly, then they can delaminate due to thermal shock (Fig. 3.5).

The input and waste reservoirs on the bonded wafers were covered with blue tack tape to prevent particulates from entering the channel. With this bonding process, very small reduction in imprinted channel height was observer (< 0.5 μm). Individual custom-shaped PMMA microchannel chip were cut out of these bonded PMMA wafers.

Wafers were also bonded using UV-ozone treatment. The surfaces of the imprinted wafer and the cover plate were UV-ozone treated for 10 minutes each. The wafers were then bonded at 90^{o}C with bonding force of 11000 lbs (48.93 kN). However, during the thermo-mechanical deformation, local flower shaped spots were observed, which can be local delamination or modification of the bond surface due to some unknown chemical reaction initiated by the UV-ozone treatment. Considerable delamination was also observed along the microchannel after thermo-mechanical deformation. This was consistently observed for all UV-ozone treated chips.

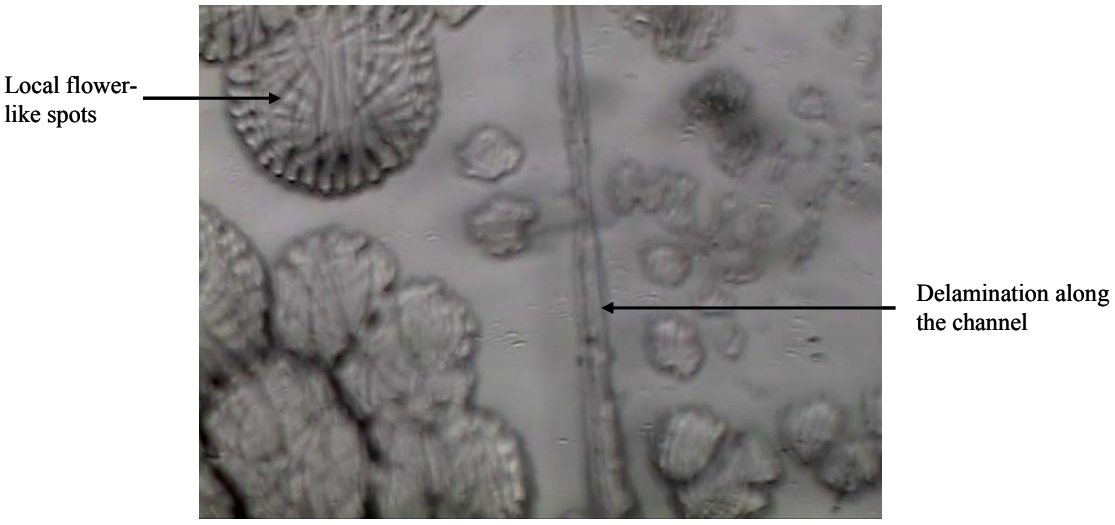

Figure 3.6 Flower-like spots in a UV-ozone treated chip after heat treatment.

3.3 Thermo-mechanical Deformation

During the thermo-mechanical deformation process, a section of the microchannel in the thermoplastic chip was constricted to nano-scale with the custom-designed, mechanical deformation rig. This process consists of two important steps, namely: individual chip cutting into a custom shape to fit in the rig (Fig. 3.7) and the chip mounting in the rig.

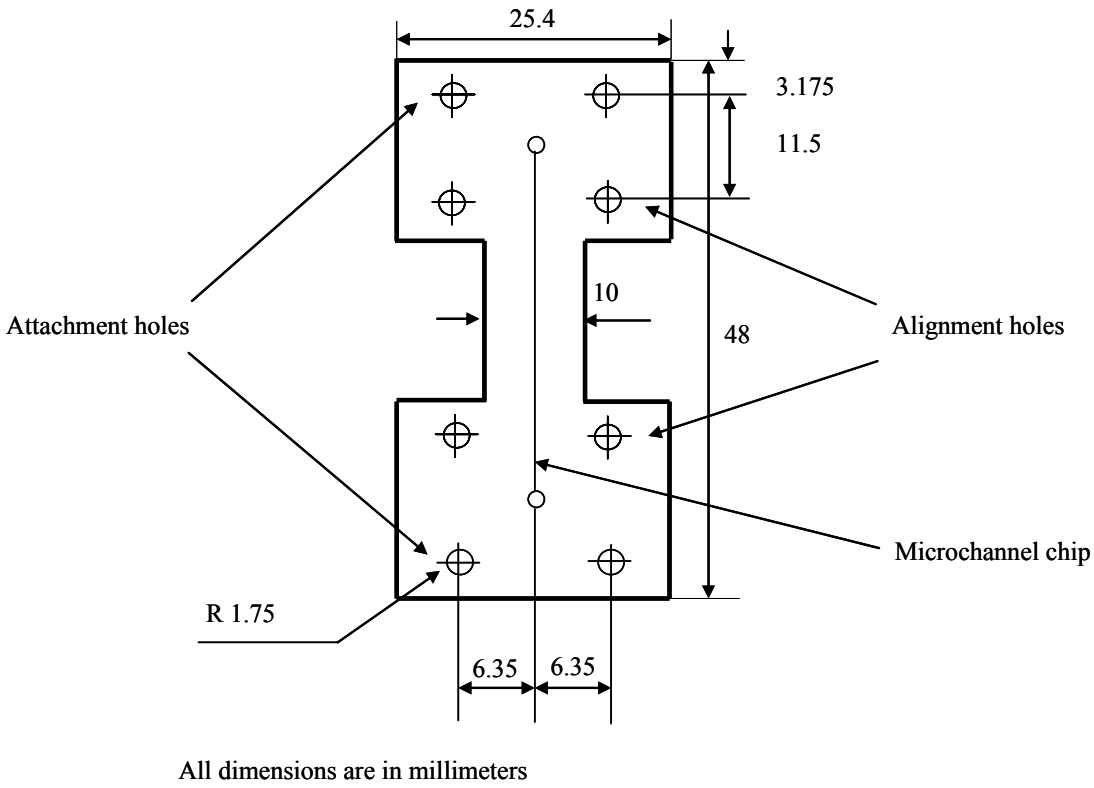

Figure 3.7 Custom-shaped plastic microchannel chip before thermo-mechanical deformation

Alignment holes and attachment holes (3.5 mm in diameter) were drilled symmetrically adjacent to the microchannel in the thermally bonded PMMA wafers. The bonded wafers were then cut into rectangular shapes (25.4 mm x 48 mm). Two slots were milled in these individual, rectangular chips so that the microchannel was located at the middle of a 10 mm section (Fig. 3.7). Milling ensured flat machined surface, which was critical for uniform compressive strain on the channel. At no applied strain condition, the parallel plate probes slide into these slots and touch the chip at the milled surfaces of the chip at equal distance from the microchannel.

3.3.1 Microchannel Chip Mounting Procedure

The custom-shaped microchannel chip was mounted between two aluminum, chip locating plates (#11, Fig. 2.12) welded at the center of top and bottom plates of the mechanical rig with the help of chip-holding plates (#5, Fig. 2.12) (Fig. 3.10). These aluminum plates were precision welded so that they are perpendicular to the top and bottom plate planes. Custom-shaped, thin, aluminum plates were sandwiched between the chip-holding plates and the microchannel chip to provide fixed boundary conditions on both faces of the chip. These thin aluminum plates are similar in shape to the microchannel chip, but with a narrower section at the center (Fig. 3.8).

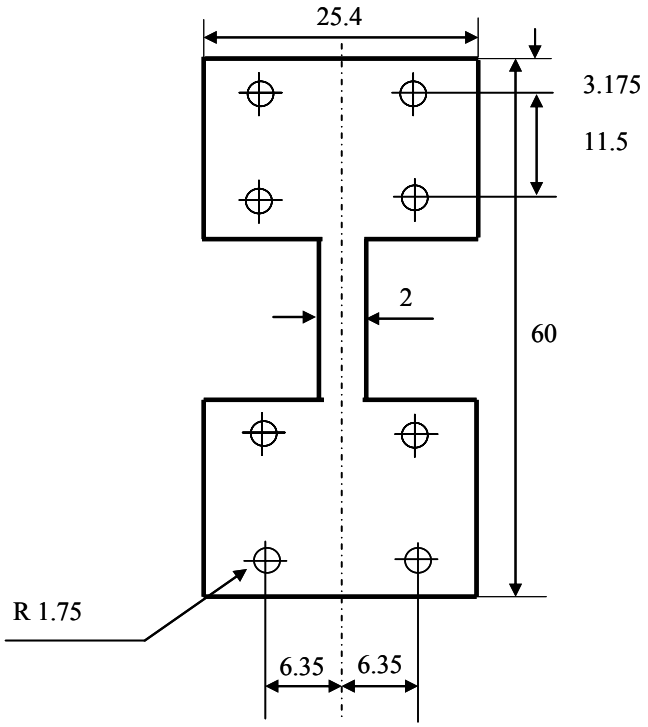

Figure 3.8 Thin aluminum plate to provide fixed boundary conditions on chip faces.

Narrower section was required to ensure that the plate probes can produce indentation and were not stopped by these aluminum plates. Thus the PMMA microchannel chip was vertically held at the center of the rig between the chip locating plates, with a holding assembly configuration of chip holding plates on the outside, followed by the thin aluminum plates for fixed boundary condition on either side of the microchannel chip and the chip at the innermost position in the sandwich (Fig. 3.9, Fig. 3.10). Following was the chip mounting procedure developed.

First ensure that the plate probes are away from the location where the microchannel chip is going to be mounted (i.e. between the chip locating plates). The displacement stopping nuts (#10, Fig. 2.12) hold the compression springs from expanding.

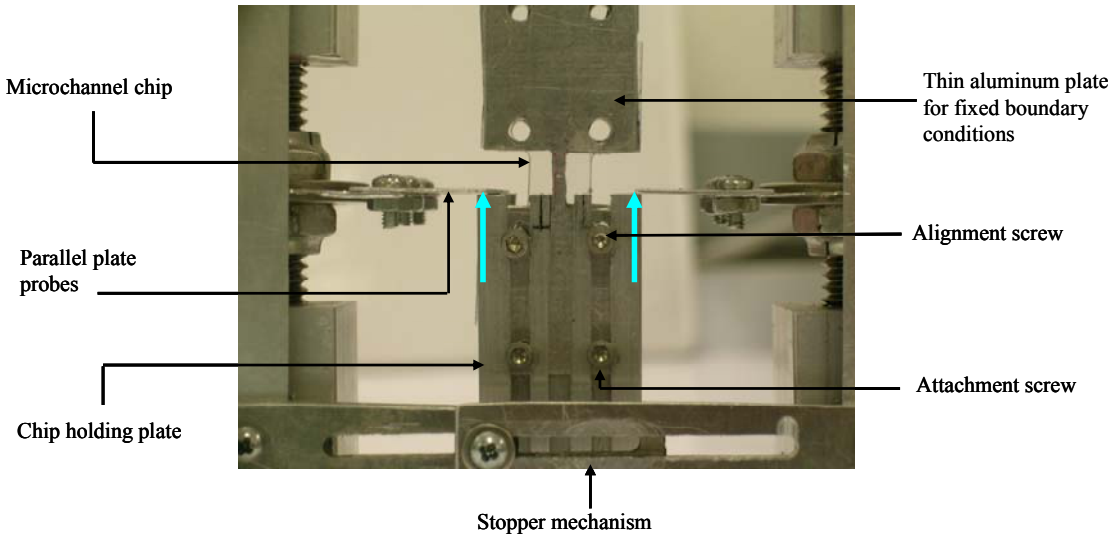

Figure 3.9 Assembly of lower chip holding plates, aluminum plates and microchannel chip.

An sandwich assembly consisting of the chip holding plates (2 in number), thin aluminum plates (2 in number) (Fig. 3.9) and the microchannel chip was aligned with the vertical chip locating plate (#11, Fig. 2.12) welded to the bottom plate with the

help of two, 1 inch long 4-40[†] screws passing through the attachment holes and two similar screws passing through the alignment holes. The chip holding plates were slid towards the parallel plate probes so that they just touch the probes. The screws through the attachment holes were tightened to firmly hold the assembly. This assembly will be below the parallel plate probes (Fig. 3.9).

A similar assembly was performed on top of the plate probes. The top and bottom chip holding plates were thus separated by a small gap in which the plate probes (#4, Fig. 2.12) slid during the expansion of the compressed springs (#2, Fig. 2.12), thus providing the necessary compressive strain in one plane (Fig. 3.10).

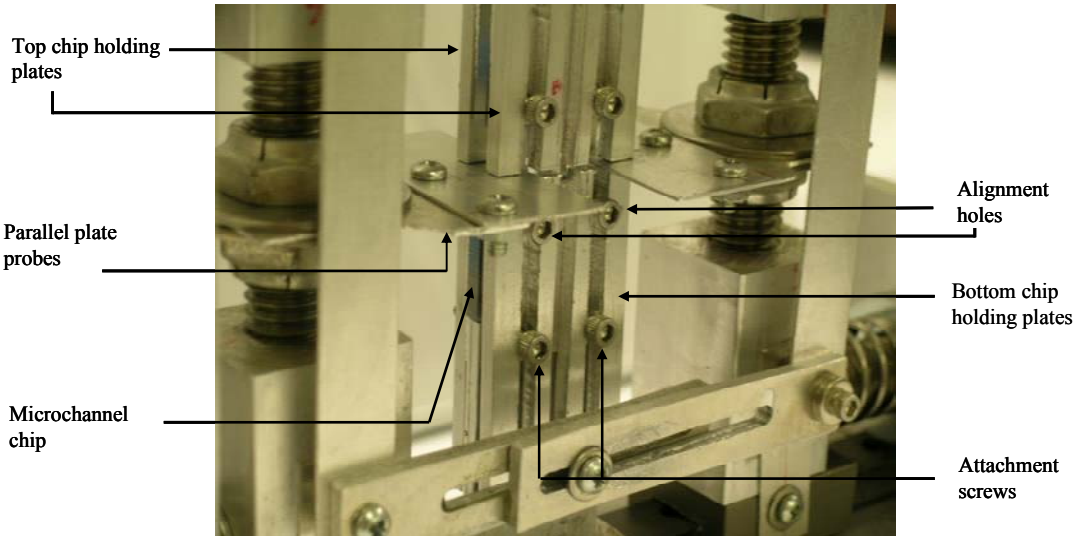

Figure 3.10 Complete assembly of vertically held chip with of chip-holding plates.

This assembly prevented/reduced any offset in deformation planes of the probes along the microchannel length, which would have caused the channel to undergo displacement/bending during deformation, thereby reducing the efficiency of the rig.

[†] Information about 4-40 type screws can be located at URL: http://www.engineersedge.com/screw_threads_chart.htm

The displacement stopping nuts on each side of the rig were rotated in anti-clockwise direction so that the compressed springs started expanding, which resulted in motion of the plate probes in the gap between the chip holding plates towards the vertically held chip.

When the plate probes touched the sides of the chip, the screw in the stopper mechanism (#6, Fig. 2.12) was tightened (Fig. 3.10). At this point, the load on displacement stopping screws will reduce considerably, as the load due to the compressed springs will be shared by the plastic microchannel chip and the stopper mechanism.

Each of the displacement stopping nuts was further rotated in anti-clockwise direction to set a displacement that needs to be provided to the plate probes during the thermo-mechanical deformation process (Fig. 3.11). One rotation of the nut on the horizontal ½"-13 threaded rod will result in 1.96 mm ≈ 2mm.

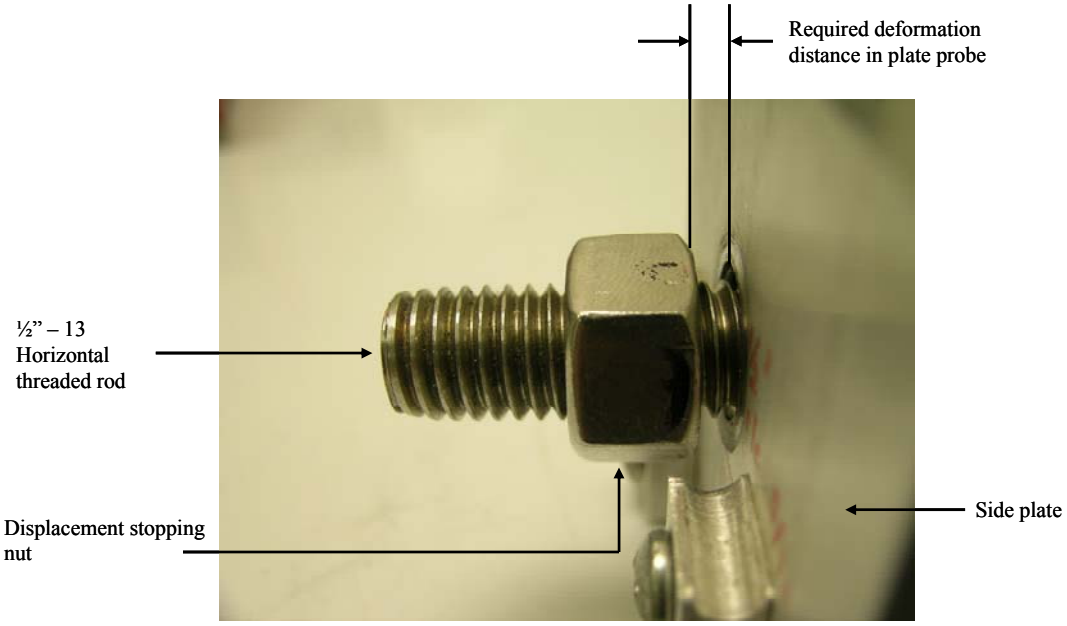

Figure 3.11 Positioned displacement stopper nut for specific indentation.

Thus, the displacement was set depending upon the required strain. The microchannel lies at the center of a 10 mm neck in the custom-shaped plastic chip (Fig. 3.7). Thus, if each of the displacement stopping nuts is placed 2 mm from the side plates (#7, Fig. 2.12), then the displacement in each plate probe will be 2 mm. As a result, the total displacement towards the microchannel will be 4 mm (2 mm in each of the plate probes), giving a compressive strain of 40 %.

After the displacement stopping nuts were set at a required position, the mechanical rig was placed in a convection oven preset at 120^{o}C. A drop in temperature of the oven was observed at this point. When the temperature in the oven again reached a steady state value of 120^{o}C, the screw in the stopper mechanism was unscrewed to loosen the stopper mechanism (approximately 110 minutes for the developed mechanical rig). The compression springs, which were held fixed due to the stopper mechanism underwent expansion, thereby providing displacement to the parallel plate probes. The expansion in the springs stopped when the displacement stopping nuts touched the side plates, thus stopping the displacement in the plate probes and only a pre-determined indentation was produced in the plastic chip.

Expansion process takes about 10 minutes. A dwell time of 10 minutes was allowed after the screw in the stopper mechanism was loosened to ensure complete thermo-mechanical deformation of the heated plastic chip. The rig was cooled down to room temperature and the deformed microchannel chip was removed from the rig.

To measure the cross-sectional dimensions of the deformed microchannel, the deformed microchannel chip was cryogenically cross-sectioned at the deformation site using liquid nitrogen. Following are the chip cross-sectioning steps followed.

- The deformed microchannel chip was milled to remove any bulge formed on top of it faces during the thermo-mechanical deformation.
- A notch was made on the face of the chip along the line of the indentation marks. The notch provided a crack initiation site. This ensured that the deformed microchannel dimensions were measured at the maximum deformation site.
- The width of the chip near the deformation site was reduced using a band-saw so that the chip shears quickly under a relatively low impact force.
- These notched chips were then annealed at 80^{o}C overnight to relieve the un-uniform stress across the chip cross section. There is stress accumulation near the microchannel after the thermo-mechanical deformation. Annealing ensures that the cross-sectional face of the chip is flat and smooth after it is sheared.
- Four, 4-40 screws were passed through the holes in the stress relieved chips and firmly tightened (Fig. 3.12). These tightening screws ensured that the chip did not delaminate due to thermal shock after removing from liquid nitrogen.
- The chip was then held in an aluminum clamp in such a fashion that the section on one side of the notch was clamped and the section on other side formed a cantilever beam-like structure. Thus, the plane of cross-section was adjacent to the aluminum clamp on the flat surface. The space between the clamp and deformation plane was such that it fit a 200 μm thick blade. (Fig. 3.12)
- The whole assembly was immersed in liquid nitrogen held in a foam container. The assembly was kept on a brass chuck already immersed in liquid nitrogen. The assembly was allowed to cool down to liquid nitrogen temperature (-196^{o}C). An indication of this is that the nitrogen bubbles, which are observed when the

assembly at room temperature is immersed in liquid nitrogen, will stop emerging out of liquid nitrogen.

- A 200 μm thick, steel blade was held in the notch made in the chip with the help of pliers. The blade is allowed to cool down to liquid nitrogen temperature.
- Using a light tack-hammer, an impact was given to the blade. This impact produced enough force to shear the chip which had become brittle after immersing in liquid nitrogen.
- The cross-sectioned chip can then be gradually brought to room temperature to prevent any delamination due to thermal shock.
- The cross-section of the chip can be observed under optical microscope or can be imaged using a scanning electron microscope.

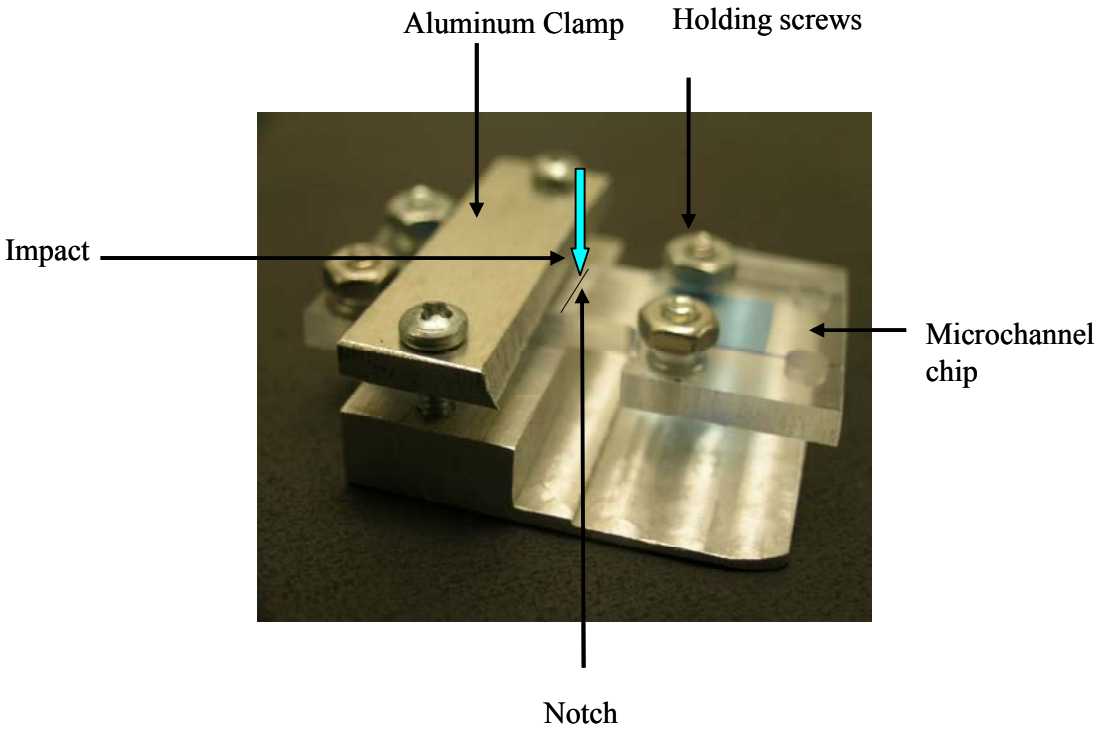

Figure 3.12 Assembly for cryogenic microchannel chip cross-sectioning.

Chapter 4: Experimental Results and Discussion

Microchannels in thermally bonded PMMA chips were thermo-mechanically deformed at 120^{o}C in a convection oven to constrict the microchannel to nanoscale. Microchannels with different aspect ratios and sizes were deformed at strains so as to reduce the microchannel width to submicrometer dimensions. Three initial microchannel cross-sectional sizes were used here, namely: 10 μm (width) x 15 μm (height) [case 1]; 10 μm (width) x 5 μm (height) [case 2]; 5 μm (width) x 3 μm (height) [case 3]. The thermo-mechanical deformation was performed with and without fixed boundary conditions on the faces of the PMMA microchannel chip for case 1 and with fixed boundary conditions for cases 2 and 3.

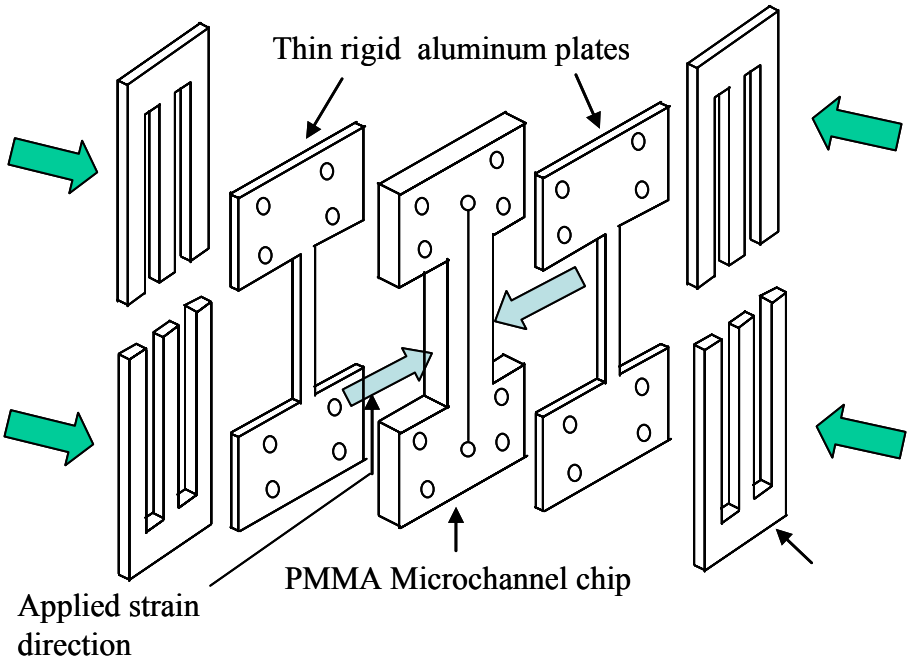

Figure 4.1 Thin aluminum plates for fixed boundary conditions on the chip faces during thermo-mechanical deformation

Thermo-mechanical deformation with fixed boundary condition implies deformation of the heated microchannel chip in the mechanical rig with the thin aluminum plates covering the faces of the chip, which are perpendicular to the strain application direction (Fig. 4.1). Thus the material in the vicinity of the channel along its length is restricted from bulging out, perpendicular to the chip's face, after deformation (see Fig. 2.1). The absence of these aluminum plates during deformation leads to deformation without fixed boundary conditions. The material thus forms a bulge along the length of the channel at the deformation region.

4.1 Case 1: Thermo-mechanical deformation of 10 μm (width) x 15 μm (height) microchannel

This high aspect ratio[†] (aspect ratio = 1.5) microchannel was deformed in such a way that the width of the microchannel reduced to sub-micrometer dimension. When the fixed boundary conditions were not applied on the faces of the microchannel chip during the thermo-mechanical deformation, it was observed that the width at the center of the microchannel decreased to sub-micrometer regime (966 nm) for a lateral, compressive strain of 30 %. Moreover, the reduction in width of the channel at its center was highest, thus giving an hour-glass shaped cross-sectional profile, as predicted by the finite element model for high aspect ratio microchannels (Fig. 4.2). Thus, the custom mechanical rig developed was capable of producing the desired effect of thermo-mechanical constriction of the microchannel to nanoscale dimensions. However, the widths at top and bottom of the microchannel remained above 1μm, thereby creating trans-micrometer sized holes. This will adversely affect the detection efficiency in

[†] Aspect ratio is the ratio of the channel height to the channel width.

applications such as single molecule detection. For example, in case of single molecule detection using this channel profile, not all the molecules passing through the nanochannel constriction will be detected by the sub-micrometer wide confocal microscope laser spot, thereby reducing the detection efficiency.

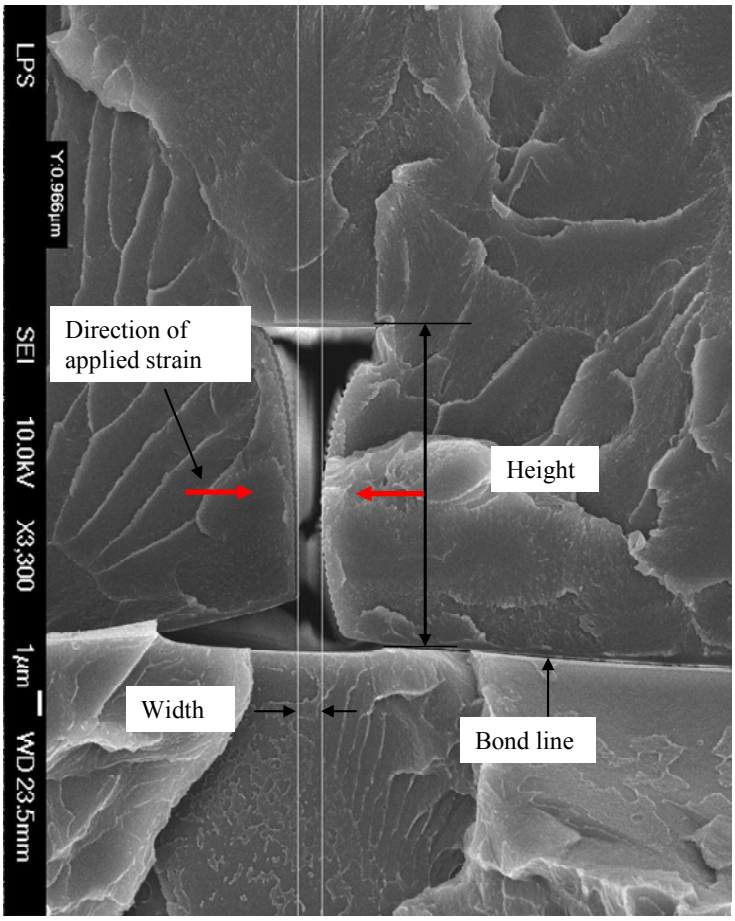

Figure 4.2 SEM image of a thermo-mechanically deformed high aspect ratio channel.

It was also observed that the top side (side away from the bond line) of the microchannel bent slightly towards the center of the channel and the bottom side away from the center of the channel, in contradiction with the model. This phenomenon was consistently observed in all the chips deformed with this setup. One of the contributing reasons could be the relative motion of the bulk material, perpendicular to the direction of

applied strain during the thermo-mechanical deformation process due to bending in the softened microchannel chip. A curvature in the bond line indicated the relative motion of bulk material cause due to bending in the chip along a preferential direction (perpendicular to face of the chip) during thermo-mechanical deformation. To make use of variable width along the height of the deformed microchannel, this high aspect ratio microchannel was subjected to higher lateral, compressive strains with an intention to close the microchannel at the center and create two, one-dimensional, triangular nanochannels, one at the top[†] and other at the bottom[††]. The microchannel chip was deformed at 60%, 70% and 80% lateral, compressive strains. It was observed that a sub-micrometer (height = 896 nm) triangular channel was obtained at the top for 70% strain (Fig. 4.4). At 60% applied strain, the channel at top had a height of 1.5 micrometers (Fig. 4.3). However, a trans-micrometer, rhombus shaped hole was also observed at the bond interface of the chip. Thus, the detection efficiency of such a cross-sectional profile will be less as most of the molecules to be detected will pass through the trans-micrometer hole, which will not be detected by the detection laser.

[†] Top indicates the position at maximum height of the imprinted channel away from the bond line.

[††] Bottom indicates the position at the bond-channel interface i.e. along the bond line of the chip.

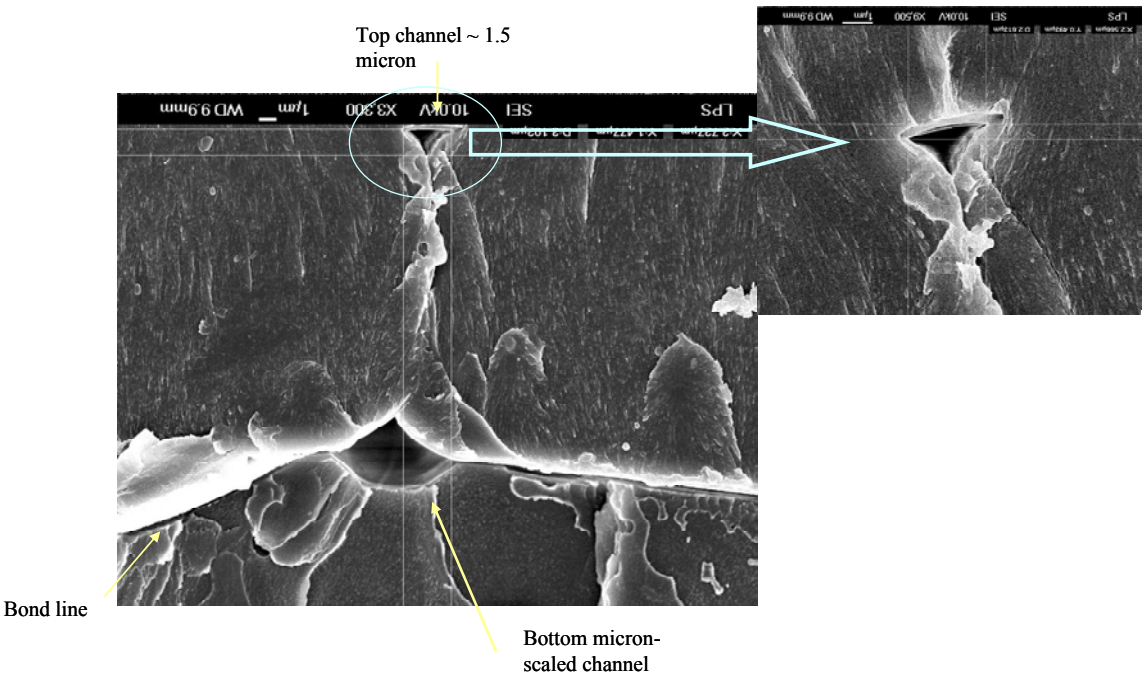

Figure 4.3 SEM image of thermo-mechanically deformed high aspect ratio channel at 60% strain.

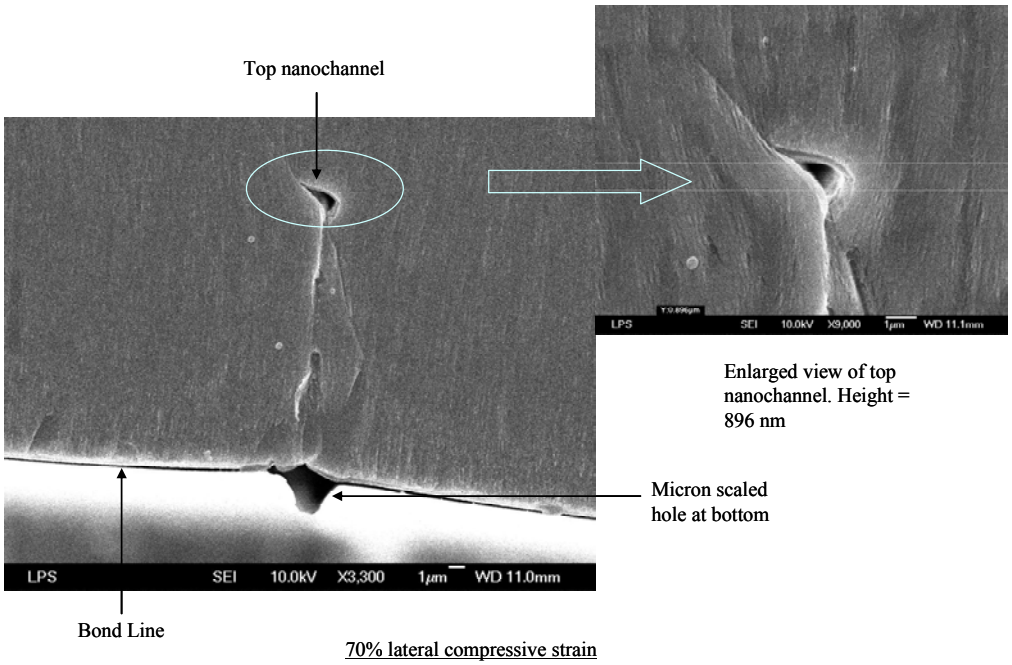

Figure 4.4 SEM image of thermo-mechanically deformed high aspect ratio channel at 70% strain.

Moreover, the production of this one-dimensional nanochannel was not consistent and for other chips deformed at 70% strain, the top triangular channel was completely closed. The variability in motion of the bulk material can be considered as a major reason for the inconsistency of the one-dimensional nanochannel production. The motion of the bulk material depends upon the it's viscosity, which in turn depends on the deformation temperature and the chip's alignment with respect to the deformation probes.

At 80% strain, the channel at top completely collapsed (Fig. 4.5). It was thus hard to control the dimensions of the channel at the top, once it reaches sub-micrometer dimensions. The rig was designed in such a way that the compressive strain can only be applied in steps of 10%. Below this value, precise indentation is not possible.

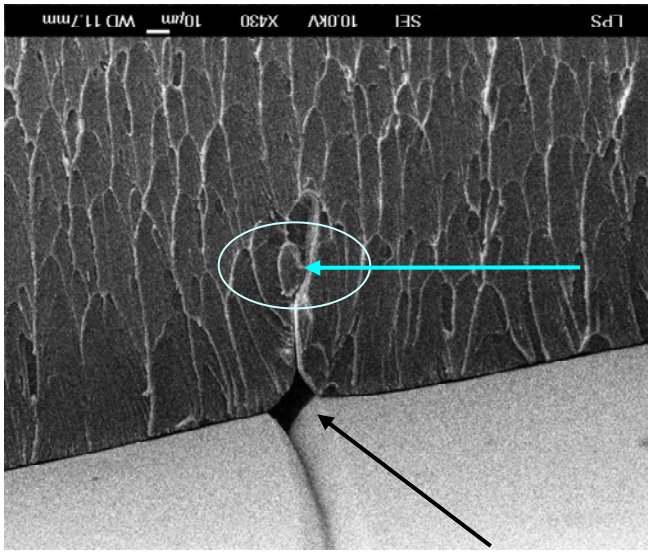

Figure 4.5 SEM image of thermo-mechanically deformed high aspect ratio channel at 80% strain

In order to restrict the bending at the bottom of the channel and obtain two sub-micrometer triangular channels, fixed boundary conditions were applied to the faces of the microchannel chip during the thermo-mechanical deformation. It was observed that the bending in the bottom side of the channel away from the channel center that was observed in absence of the boundary conditions, was restricted. But at the same time, the top horizontal side of the channel bent more inwards towards the channel center, thereby closing the channel at the top. A trans-micrometer, trapezoidal channel was developed (Fig, 4.6). Channel with such a cross-section cannot be efficiently used for single molecule detection as the nanochannel volume does not match the laser detection volume.

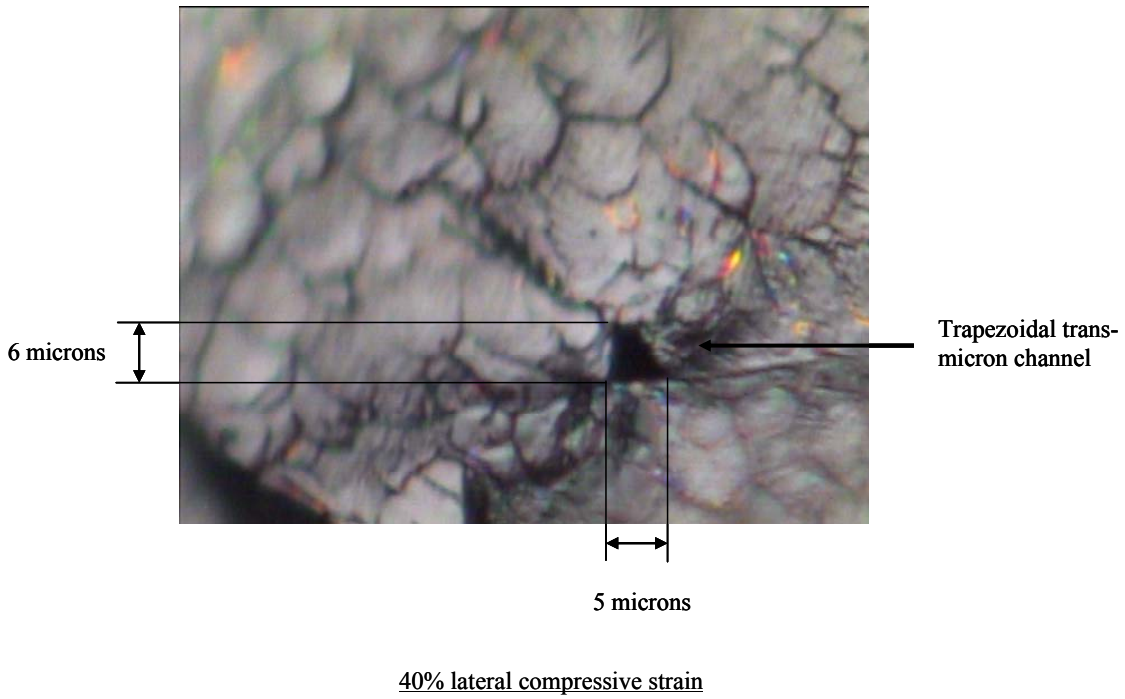

Figure 4.6 Trapezoidal cross-section of thermo-mechanically deformed high aspect ratio channel with fixed boundary conditions.

Similar results were obtained for 50% applied strain. One of the reasons for the variable deformation characteristics in top and bottom side of the microchannel can be stress concentration near the imprinted channel and at the bond interface. The top side of the microchannel, which is the horizontal side of the imprinted channel, suddenly collapsed under the action of the applied strain. In case of the bottom side, which was provided by the cover-slip after thermal bonding, there could have been a stress accumulation at the bond interface on either side of the bottom side of the microchannel. On the other hand, there would be no stress on the bottom side. This stress distribution across the channel cross-section may be the contributing factor for this irregular deformation nature.

Moreover, for a higher aspect ratio channel, there was a considerable decrease in dimensions of the channel for small changes in the applied strain. Thus, smaller irregularities in applied strain, in terms of uniformity of the strain on either side of the channel, misalignment of the plate probes with respect to the microchannel would have adversely affected the deformation dynamics of the microchannel. A combined effect of the above two causes may have lead to irregular deformation of the microchannel.

4.2 Case 2: Thermo-mechanical deformation of 10 μm (width) x 5 μm (height) microchannel.

A microchannel with cross-sectional dimensions, 10 μm (width) x 5 μm (height) was subjected to lateral, compressive strains varying from 40% to 70%, in steps of 10% with fixed boundary conditions on the chip faces. The deformation temperature is 120^{o}C.

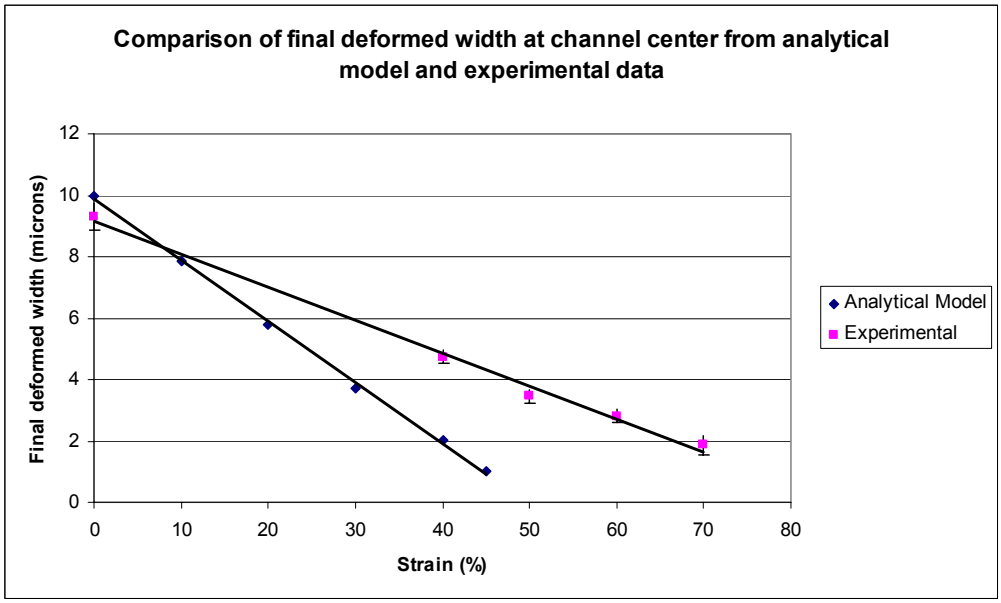

Figure 4.7 Comparison of experimental and theoretical final deformed microchannel widths

It was observed that the microchannel reduced in all directions, which corroborates the proposed theory in chapter 2 (indicated by bold black arrows in fig. 4.8). The width reduced to an average value of 1.85 μm from 10 micrometer initial width at a strain of about 70%. On the other hand, the height of the channel reduced to around 0.8 μm from 5 micrometers. When the experimental results were compared with the model results, it was observed that the actual strain required for the channel to reduce to nano-scale or near sub-micrometer dimensions is much larger than theoretical strain (>70% actual strain as compared to 42% in case of model) (Fig. 4.7). This discrepancy between the actual and theoretical values can be attributed to the viscous flow of the material during thermo-mechanical deformation. The model assumes an elastic behavior for the deformation process at low applied strains. However, during the thermo-mechanical deformation process, there is viscous flow of the material indicating viscoplastic behavior at higher strains. The fixed boundary conditions on the faces of the chip prevented any

bulk material motion perpendicular to the faces of the chip in the region close to the microchannel during this viscous flow. This offered resistance to the bulk flow of the material towards the microchannel. As a result, the viscous material takes the least flow-resistance path and forms bulges on either side of the fixed boundary condition plates. This reduced bulk material flow of the material towards the channel reduced the efficiency of the rig (i.e. higher strains required to reach sub-micrometer width). Thus a larger strain was required to reduce the microchannel width to near micrometer dimension.

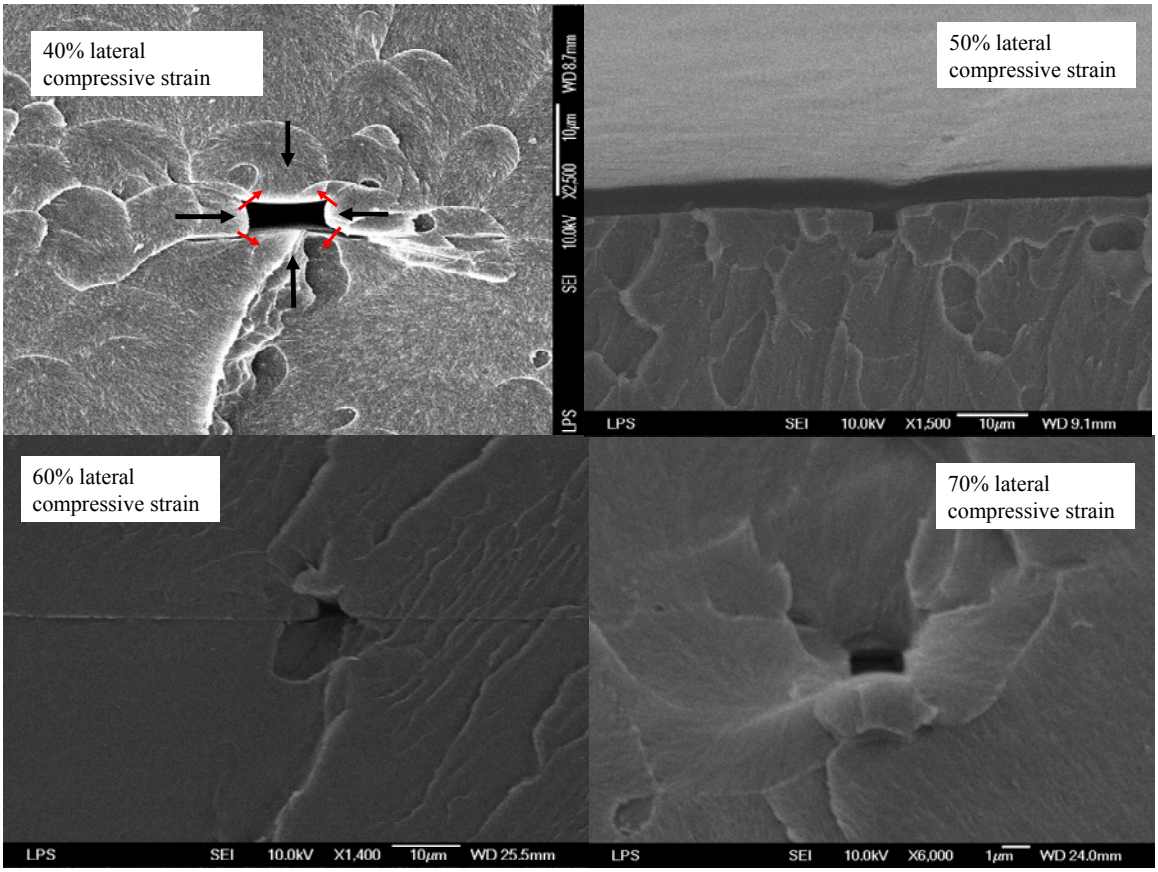

Figure 4.8 SEM image of thermo-mechanically deformed channel at different compressive strains

Isotropic material properties were assumed in the model. The material properties might not be isotropic depending upon its composition. This could have also affected the deformation dynamics of the microchannel.

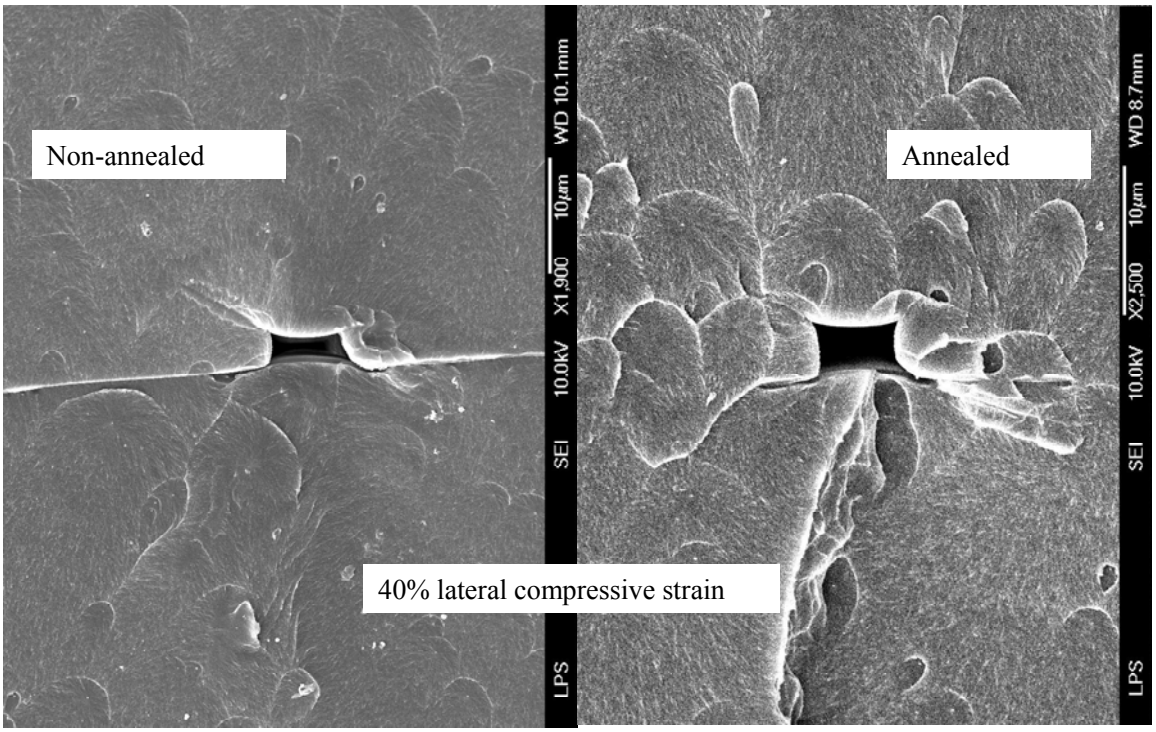

Figure 4.9 Comparison of thermo-mechanically deformed cross-section for annealed and non-annealed chips.

It was also observed that annealing a thermally bonded chip with an embossed channel improved the deformation performance. Annealed and non annealed chips were deformed at same strains, 40% and 50%. The annealed chips showed a greater reduction in width of the channel as compared to non-annealed chips.

4.3 Case 3: Thermo-mechanical deformation of 5 μm (width) x 3 μm (height) microchannel.

To allow the channel width reach sub-micrometer dimensions at lower strains, a microchannel in the PMMA chip with cross-sectional dimensions of 5 micrometers (width) and 3 micrometers (height) was thermo-mechanically deformed at 120^{o}C. Reduction in all the dimensions of the channel was observed as in the previous case. A minimum average width of 1.758 μm was observed for an applied strain of 50 %. The corresponding average height for 50% strain is 1.43 μm (Fig. 4.10, Fig. 4.11). Similar to case 2, a larger strain is required for the microchannel width to reduce to close to 1 μm when compared to theoretical strain predicted by the model. When the microchannel with these initial dimensions was subject to 60 % compressive strain, the width at the center of the channel reduced below one micrometer (625 nm) (Fig. 4.11). When microchannel with these initial cross-sectional dimensions was further deformed at 70% strain, the deformed channel was observed to be collapsed. This was consistently observed for all the chips deformed at 70% strain (Fig. 4.12). The fabrication method is thus limited in its ability to precisely control the width of the deformed channel within 1 micrometer range. This can be attributed to the limited least count of strain application. Lateral compressive strain in steps of 10 % can be applied using the mechanical rig developed. If precise control (< 10% resolution) in strain application is achieved in the mechanical rig, then the final width of the deformed microchannel can be controlled efficient below 1 micrometer. Moreover, error in manufacturing individual chips for deformation, like width of the narrow section of the individual chip less than 10 mm, could have lead to larger strain induced into the chip than actual strain applied, which could have resulted in channel collapse.

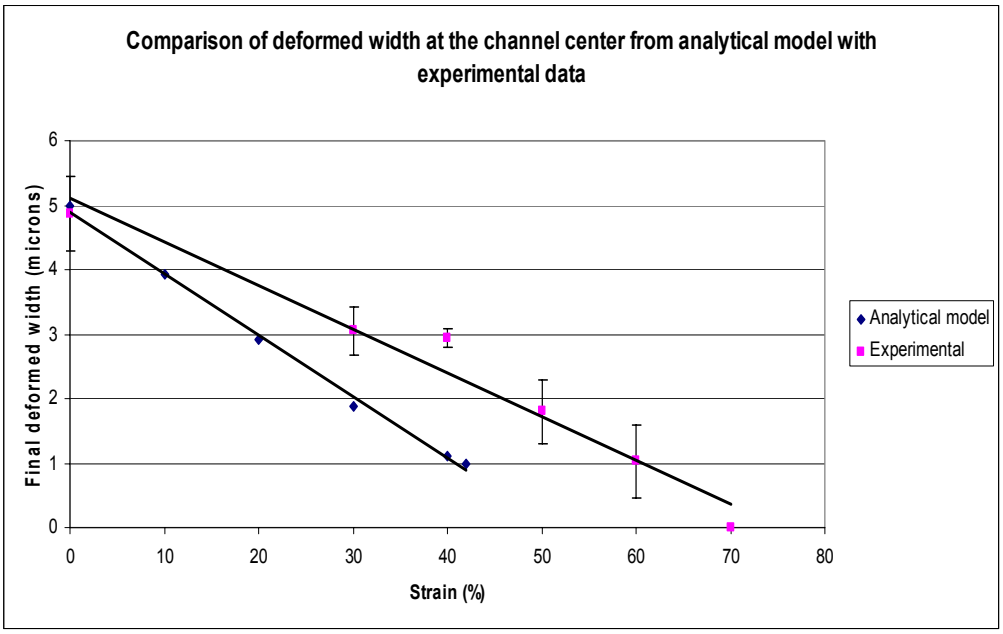

Figure 4.10 Comparison of theoretical and experimental deformed microchannel widths.

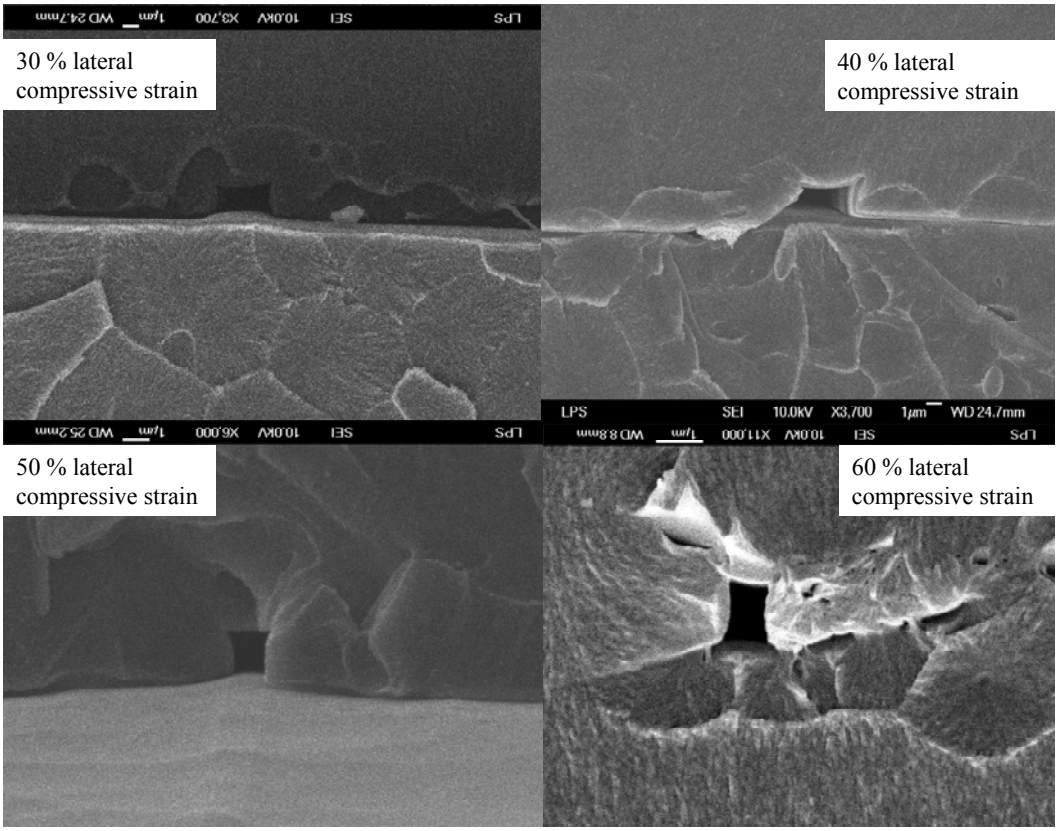

Figure 4.11 SEM images of thermo-mechanically deformed microchannel at various compressive strains

The possible cause for this difference in required strain as predicted by the model and actual required strain is same as explained above. However, a final width below 1 micrometer was observed at a lower strain (60%) in case 3 as compared to the case 2 (70 %). Moreover, the microchannel width did not reduce below 1 micrometer for case 2. When the reduction in height for the above two cases was compared, it was seen that the reduction in height of the channel in case of the 10 µm (width) x 5 µm (height) channel is more than 5 µm (width) x 3 µm (height) channel. The initial width of the microchannel in case 2 was greater than case 3, which allows the top and bottom sides of the microchannel to bend more at center under the action of applied strain. Thus in case 2, in which the width of the microchannel reduced from 10 µm to around 1 micrometer dimension, a larger bending in top and bottom sides occurred, resulting in smaller height of the deformed microchannel as compared to the case 3.

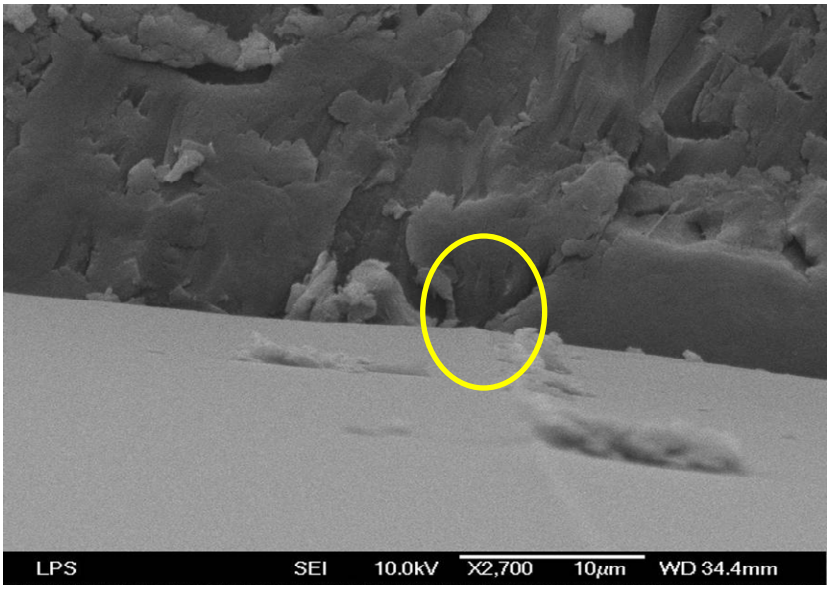

Figure 4.12 Collapsed microchannel after thermo-mechanical deformation at 70% strain

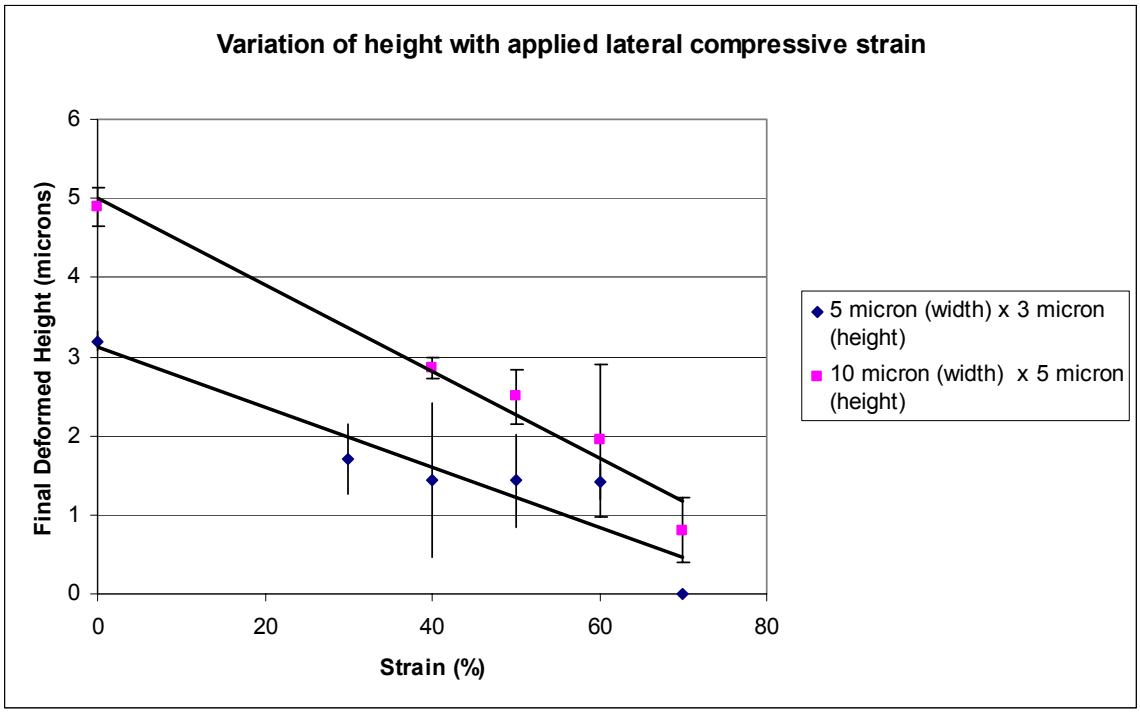

Figure 4.13 Comparison between reduction in heights for cases 2 and 3.

It was observed that the reproducibility of the fabrication method worsened for higher deformation strains, as indicated by the increasing variance of the final deformed width measurements. This can be attributed to the variable viscous flow dynamics of the thermoplastic material during thermo-mechanical deformation. The uniformity in the flow of the material depends on the thermoplastic chip alignment accuracy with respect to the probes. Any misalignment, even minute, could have produced an amplified effect on the flow behavior at higher strains leading to inconsistent flow of the material. It was observed after thermo-mechanical deformation that in some of the deformed chips, the microchannel had collapsed whereas in some cases the deformation in microchannel was much less than expected. This anomalous behavior can be attributed to the inconsistent material flow dynamics as explained above along with manufacturing errors and assembly misalignments.

It can be inferred that in order to obtain a sub-micrometer wide channel from a rectangular initial microchannel, it is necessary to start with a low aspect ratio channel (width > height) with small initial dimensions. However, if the initial width of the microchannel is reduced to extremely small values, then the corresponding initial height should be further reduced. There is a limitation to doing this, as the enclosed microchannel is formed by thermal bonding procedure and shorter channels are prone to collapse during this process.

Chapter 5: Summary

A novel fabrication process to develop a nanochannel from a microchannel with a rectangular cross-section, using thermo-mechanical deformation of thermoplastic chip containing that microchannel was evaluated in this thesis. The effects of shape and size of the initial microchannel on the deformation dynamics and final deformed microchannel dimensions were studied. A 2D, plane strain finite element model was developed in ANSYS® to estimate the deformation conditions required to deform microchannels with different shapes and sizes to sub-micrometer dimensions. A proof of concept was performed by mechanically deforming a PDMS microchannel to sub-micrometer dimensions.

Various thermo-mechanical deformation approaches were evaluated to heat the microchannel chip and then produce specific mechanical deformation in the heated chip. This lead to the design of a compact, custom mechanical rig to produce the thermo-mechanical deformation in the microchannel chip. The developed mechanical rig was optimized to produce the desired mechanical constriction effect on the microchannel. Microchannels with two different shapes and three different sizes in PMMA chips were thermo-mechanically deformed.

It was observed that the required compressive deformation strain and the final deformed channel dimensions depended on the aspect ratio (shape) and the size of the microchannel. For higher aspect ratio microchannel, lower strains were required to reach sub-micrometer dimensions. However, the final deformed width of the microchannel varied considerably along its height and trans-micrometer openings were obtained along with a sub-micrometer width section across a cross-section of the

deformed microchannel. The deformation was more sensitive to applied strain for high aspect ratio microchannels and thus precise control of deformed microchannel dimensions was impossible using the developed mechanical rig. As the aspect ratio was reduced, the strain required to deform the width of the microchannel to near micrometer dimensions increased. However, the required strain strongly depended on the size of the channel. For smaller microchannels with nearly the same aspect ratio, the strain required to reach near/sub micrometer widths was about 10% less than for bigger channels. Thus, it is recommended to deform a low aspect ratio microchannel with low initial cross-sectional dimensions. But the size of the microchannel is limited by the lithography limitations and the thermal bonding process.

The consistency and efficiency of the fabrication process demonstrated was prone to manufacturing and assembly tolerances. The final deformed microchannel dimensions strongly depended upon and was extremely sensitive to the orientation of the chip in the mechanical rig, location and perpendicularity of the microchannel with respect to the deformation probes, width of the fixed boundary condition plates. Possible designs to eliminate or reduce these limitations are discussed in chapter 5.2.

5.1 Contributions

- Developed a finite element model to understand the deformation behavior of microchannels with rectangular cross-section with different shapes and sizes and to predict the deformation conditions for the microchannel width to reach sub-micrometer dimensions.
- A custom mechanical rig was designed, developed and optimized to hold the microchannel chip and to produce a specific thermo-mechanical deformation in

the chip to constrict a section of microchannel to near/sub-micrometer dimensions.

- Deformation behavior of microchannels with different shapes and sizes under the action of applied compressive strain was studied along with its effect on final deformed microchannel dimensions. Recommendations on optimum microchannel dimensions and deformation conditions were made.

5.2 Future Work

A ground-work for generation of nanochannel in polymer microfluidics chip was performed in this thesis. There are limitations to using a rectangular cross-section of the microchannel such as the variation in width of the deformed microchannel along its height and the dependence of the final deformed channel dimensions on the shape and size of the microchannel. Hence, different initial cross-sectional shapes of the microchannel should be explored which may eliminate problems faced in case of a rectangular microchannel as explained above. Some of the examples of microchannel cross-sectional shapes are rhombus or oval, which are broad at center and get narrower towards the top and bottom. It was observed that the reduction in width of the rectangular microchannel was maximum at its center under the action of applied, lateral compressive strain. Thus microchannels with rhombus or oval shaped cross-sections will deform is such a way that after thermo-mechanical deformation, there will not be any trans-micrometer opening in the deformed microchannel cross-section. Thus, the requirement of fixed boundary conditions can be eliminated and the problems encountered due to bending in top and bottom side of the rectangular microchannels can also be eliminated.

This will also reduce the strain required to reach sub-micrometer dimensions. However, the fabrication of rhombus or oval shaped microchannels in thermoplastic fluidic chip is not trivial and considerable exploration will be needed in this field.

The current mechanical deformation rig design can be modified to eliminate the out of plane bulk material flow and force all the material to flow towards the microchannel during the thermo-mechanical deformation process. Thus potential sub-micrometer wide channels can be obtained at lower, applied compressive strains. Following is a design based on this idea (Fig. 5.1).

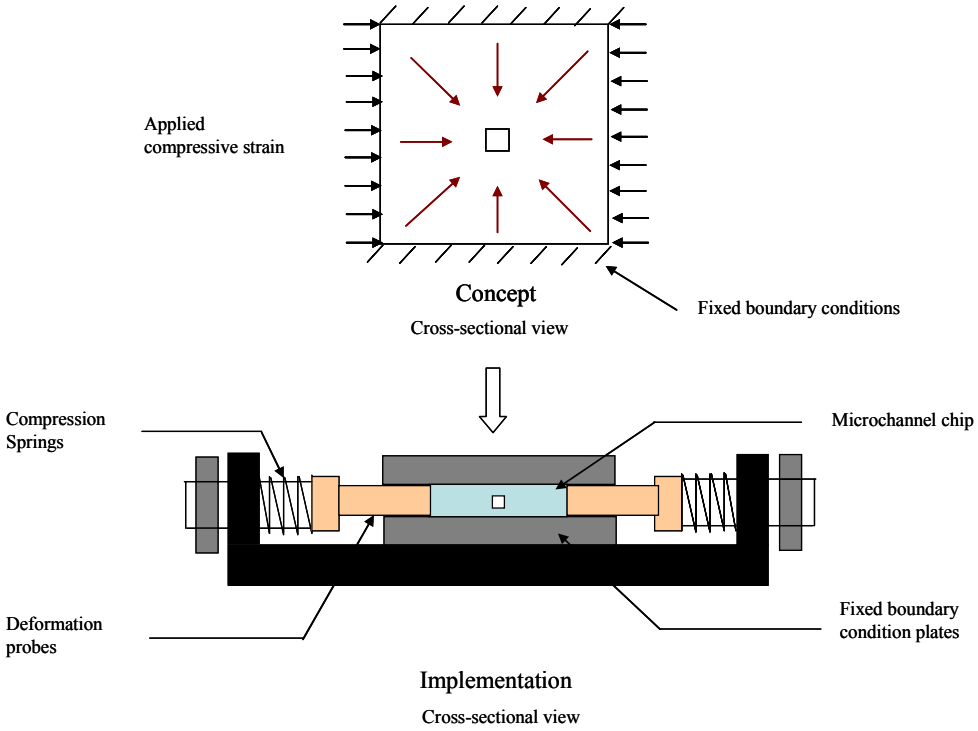

Figure 5.1 Modified mechanical rig design for higher deformation efficiency.

In this modified rig design, the fixed boundary conditions completely cover the faces of the microchannel to prevent any material from bulging out of plane of the chip. Thus, all the material will be forced to move towards the channel under the action of applied compressive strain.

Another area of exploration is the deformation temperature. The deformation temperature can be reduced so as to increase the elastic modulus of the chip material. Thus, lower strains will be required to reduce the width of rectangular microchannel to sub-micrometer regime. However, it should be noted that large deformation force will be required to produce deformation in the chip.

The model should be modified to account for the viscoplastic behavior of the thermoplastic chip to better model the actual deformation conditions.

References

[1] Alexe, M., C. Harnagea, Hesse, D. "Non-conventional micro- and nanopatterning techniques for electroceramics." Journal of Electroceramics, Vol. 12, No.1-2, Jan-Mar 2004, pp. 69-88

[2] Becker, H. and C. Gartner. "Polymer microfabrication methods for microfluidic analytical applications." Electrophoresis, Vol.21, No.1, Jan 2000, pp. 12-26.

[3] Bilenberg, B., S. Jacobsen, et al. "High resolution 100 kV electron beam lithography in SU-8." Microelectronic Engineering, Vol.83, No. 4-9, Apr-Sep 2006, pp. 1609-1612.

[4] Chang, T. H. P. "Proximity effect in electron-beam lithography." Vacuum Science and Technology, Vol. 12 No.6, 1975, pp. 1271-1275.

[5] Chapman, H. N., A. K. Ray-Chaudhari, et al. "First lithographic results from the extreme ultraviolet Engineering Test Stand." Vacuum Science and Technology, Vol. 19, No.6, 2001, pp. 2389-2395.

[6] Chen, W. and H. Ahmed. "Fabrication of 5–7 nm wide etched lines in silicon using 100 keV electron-beam lithography and polymethylmethacrylate resist." Applied Physics, Vol.62, No.13, 2001, pp.1499-1501.

[7] Chou, S. Y., P. R. Krauss, et al. "Nanoimprint lithography." Journal of Vacuum Science & Technology B (Microelectronics and Nanometer Structures), Vol.14, No.6, 1996

[8] Guarini, K. W., C. T. Black, et al. "Nanoscale patterning using self-assembled polymers for semiconductor applications." Vacuum Science and Technology B, Vol.19, NO.6, October 2001, pp. 2784-2788.

[9] Haneveld, J., H. Jansen, et al. "Wet anisotropic etching for fluidic 1D nanochannels." Journal of Micromechanics and Microengineering, Vol. 13, No.4, July 2003, pp. S62-S66.

[10] Harnett, C. K., G. W. Coates, et al. "Heat-depolymerizable polycarbonates as electron beam patternable sacrificial layers for nanofluidics." Journal of Vacuum Science & Technology B (Microelectronics and Nanometer Structures), Vol.19, No.6, 2001.

[11] Kameoka J., Jing N., et al Nanochannels for the identification of single molecules. SPIE Newsroom, The International Society of Optical Engineers, 2006.

[12] Kaige, W., W. Pengye, et al. Fabricating nanofluidic channels and Applying it for single bio-molecule study. Engineering in Medicine and Biology 27th Annual Conference, Shanghai, China, Proceedings of the 2005 IEEE, 2005

[13] Kim, E., Y. N. Xia, et al. "Micromolding in capillaries: Applications in materials science." Journal of the American Chemical Society, Vol.118, No.24, June 1996, pp. 5722-5731.

[14] Kim, S. O., H. H. Solak, et al. "Epitaxial self-assembly of block copolymers on lithographically defined nanopatterned substrates." Nature, Vol.424, No. 6947, July 2003, pp. 411-414.

[15] King, K. R., W. Chiaochun, et al. "Biodegradable polymer microfluidics for tissue engineering microvasculature." BioMEMS and Bionanotechnology. Symposium (Materials Research Society Proceedings, Vol.729, 2002.

[16] Kovacs, G. T. A.Micromachined Transducers Sourcebook, WCB McGraw-Hill, 1998.

[17] Kutchoukov, V. G., F. Laugere, et al. "Fabrication of nanofluidic devices using glass-to-glass anodic bonding." Sensors and Actuators a-Physical, Vol. 114, No.2-3, Sept 2004, pp. 521-527.

[18] Kutchoukov, V. G., L. Pakula, et al. "Fabrication of nanofluidic devices in glass with polysilicon electrodes." Sensors and Actuators a-Physica,l Vol.123-24, Sept 2005, pp. 602-607.

[19] Mali, P., A. Sarkar, et al. "Facile fabrication of microfluidic systems using electron beam lithography." Lab on a Chip, Vol. 6, No.2, Feb 2006, pp.310-315.

[20] Mao, P. and J. Han "Fabrication and characterization of 20 nm planar nanofluidic channels by glass–glass and glass–silicon bonding." Lab on a chip, Vol.5, June 2005, pp. 837-844.

[21] Mijatovic, D., J. C. T. Eijkel, et al. "Technologies for nanofluidic systems: top-down vs. bottom-up—a review." Lab on a chip, Vol.5, No.5, 2005, pp.492-500.

[22] Mullenborn, M., H. Dirac, et al. "Silicon Nanostructures Produced by Laser Direct Etching." Applied Physics Letters, Vol. 66 No. 22, May 1995, pp. 3001-3003.

[23] Naulleau, P., K. A. Goldberg, et al. "Sub-70 nm extreme ultraviolet lithography at the Advanced Light Source static microfield exposure station using the engineering test stand set-2 optic." Journal of Vacuum Science & Technology B, Vol. 20 No. 6, Nov-Dec 2002, pp. 2829-2833.

[24] Noerholm, M., H. Bruus, et al. "Polymer microfluidic chip for online monitoring of microarray hybridizations." Lab on a Chip , Vol. 4 No. 1 2004, pp. 28-37.

[25] O'Brien II, M. J., P. Bisong, et al. "Fabrication of an integrated nanofluidic chip using interferometric lithography." Vacuum Science and Technology, Vol. 21 No. 6, 2003, pp. 2941-2945.

[26] Park, M., C. Harrison, et al. "Block copolymer lithography: Periodic arrays of similar to 10(11) holes in 1 square centimeter." Science, Vol. 276, No. 5317, May 1997, pp. 1401-1404.

[27] Shao, P. E., A. van Kan, et al. "Fabrication of enclosed nanochannels in poly(methylmethacrylate) using proton beam writing and thermal bonding." Applied Physics Letters, Vol.88, No. 9, Feb 2006.

[28] Sivanesan, P., K. Okamoto, et al. "Polymer nanochannels fabricated by thermomechanical deformation for single-molecule analysis." Analytical Chemistry, Vol.77, No. 7, April 2005, pp. 2252-2258.

[29] Stoykovich, M. P., M. Muller, et al. "Directed assembly of block copolymer blends into nonregular device-oriented structures." Science, Vol. 308, No. 5727, June 2005, pp. 1442-1446.

[30] Sundararajan, N., D. Kim, et al. "Microfluidic operations using deformable polymer membranes fabricated by single layer soft lithography." Lab on a chip, Vol.5, Feb 2005, pp. 350-354.

[31] T. Basché, Moerner W. E., et al. Single-Molecule Optical Detection, Imaging and Spectroscopy. Weinheim, Germany, VCH Verlagsgesellschaft mbH, 1997, pp. 223-225.

[32] Terry, S. C., J. H. Jerman, et al. "Gas-Chromatographic Air Analyzer Fabricated on a Silicon-Wafer." IEEE Transactions on Electron Devices, Vol. 26, No. 12, 1979, pp. 1880-1886.

[33] Turner, S. W., A. M. Perez, et al. "Monolithic nanofluid sieving structures for DNA manipulation." Journal of Vacuum Science & Technology B, Vol.16 No. 6, Nov-Dec 1998, pp. 3835-3840.

[34] Whitesides, G. M. and J. C. Love. The art of building small. Scientific American, 2001, pp. 39-47.

[35] Wilbur, J. L., A. Kumar, et al. "Microcontact printing of self-assembled monolayers: applications in microfabrication." Nanotechnology, Vol.7, 1996, pp. 452-457.

[36] Xia, D. Y. and S. R. J. Brueck. "Fabrication of enclosed nanochannels using silica nanoparticles." Journal of Vacuum Science & Technology B, Vol. 23, No. 6, Nov-Dec 2005, pp. 2694-2699.

[37] Zhou, O., H. Shimoda, et al. "Materials science of carbon nanotubes: Fabrication, integration, and properties of macroscopic structures of carbon nanotubes." Accounts of Chemical Research, Vol. 35, No. 12, Dec 2002, pp. 1045-1053.